A phenomenological model for the responses of auditory-nerve fibers: I. Nonlinear tuning with compression and suppression

Xuedong Zhang
Hearing Research Center and Department of Biomedical Engineering, Boston University, Boston, Massachusetts 02215

Michael G. Heinz
Hearing Research Center and Department of Biomedical Engineering, Boston University, Boston, Massachusetts 02215 and Speech and Hearing Sciences Program, Massachusetts Institute of Technology, Cambridge, Massachusetts 02139

Ian C. Bruce
Department of Biomedical Engineering, Johns Hopkins University, Baltimore, Maryland 21205

Laurel H. Carney[a)]
Hearing Research Center and Department of Biomedical Engineering, Boston University, Boston, Massachusetts 02215

(Received 20 June 2000; accepted for publication 8 November 2000)

A phenomenological model was developed to describe responses of high-spontaneous-rate auditory-nerve (AN) fibers, including several nonlinear response properties. Level-dependent gain (compression), bandwidth, and phase properties were implemented with a control path that varied the gain and bandwidth of tuning in the signal-path filter. By making the bandwidth of the control path broad with respect to the signal path, the wide frequency range of two-tone suppression was included. By making the control-path filter level dependent and tuned to a frequency slightly higher than the signal-path filter, other properties of two-tone suppression were also included. These properties included the asymmetrical growth of suppression above and below the characteristic frequency and the frequency offset of the suppression tuning curve with respect to the excitatory tuning curve. The implementation of this model represents a relatively simple phenomenological description of a single mechanism that underlies several important nonlinear response properties of AN fibers. The model provides a tool for studying the roles of these nonlinearities in the encoding of simple and complex sounds in the responses of populations of AN fibers. © *2001 Acoustical Society of America.* [DOI: 10.1121/1.1336503]

PACS numbers: 43.64.Bt, 43.64.Pg [BLM]

I. INTRODUCTION

Phenomenological models for auditory-nerve (AN) responses provide a useful tool for studying the representation of simple and complex sounds at the first level of neural coding in the auditory system. These models allow hypothesis testing of the mechanisms that underlie various response properties. They also provide a tool for creating population responses that can be used to quantify the information available to the central nervous system (CNS) for different stimuli. In this study, a phenomenological model for AN responses was developed that focuses on several nonlinear response properties of AN fibers. The motivation for the development of this model was to provide a more accurate and quantitative description of the responses of AN fibers to complex sounds, such as noise-masked stimuli and speech sounds. To study the encoding of complex stimuli, inclusion of nonlinear interactions between frequency components in the stimulus is important.

Nonlinearities that are the focus of this study include the compressive changes in gain and bandwidth as a function of stimulus level, the associated changes in the phase of phase-locked responses, and two-tone suppression. These phenomena have all been related to a single mechanism in the inner ear, often referred to as the cochlear amplifier (Patuzzi and Robertson, 1988; Patuzzi, 1996; Holley, 1996). The challenge of the present study was to develop a model with a single mechanism that produces these different response properties. The development of the model was guided by the data available in the literature, where possible. However, physiological descriptions of nonlinear response properties typically focus on one or two properties at a time, and have been conducted in a number of different species. Therefore, the goal of the present study was to develop a model that captures the key features of several AN nonlinearities, while keeping the model as simple as possible.

Evidence for nonlinear gain in the inner ear was first described in terms of a compressive nonlinearity, or reduction in gain as stimulus level was increased to relatively high levels (Rhode, 1971). More recent studies have demonstrated that the compressive nonlinearity affects responses from as

[a)]Address for correspondence: Laurel H. Carney, PhD, Department of Biomedical Engineering, 44 Cummington St., Boston, MA 02215. Electronic mail: carney@bu.edu

low as 20 dB SPL up to the highest levels tested (110 dB SPL) in the most sensitive ears (Ruggero *et al.*, 1997). Ruggero *et al.* (1992) and Cooper and Rhode (1996) showed that the compressive nonlinearity and two-tone suppression are both affected by the same experimental manipulations, providing evidence that these two nonlinear properties are likely to be due to a single mechanism. Two-tone suppression has previously been described in a number of studies of the AN (e.g., Sachs and Kiang, 1968; Costalupes *et al.*, 1987; Javel *et al.*, 1978, 1983; Delgutte, 1990; Temchin *et al.*, 1997), inner hair cells (IHCs) (Cheatham and Dallos, 1989, 1990, 1992; Nuttall and Dolan, 1993), and basilar membrane (BM) (e.g., Ruggero *et al.*, 1992; Nuttall and Dolan, 1993; Rhode and Cooper, 1993, 1996; Cooper, 1996). Two-tone suppression grows with suppressor tone level at different rates depending upon the frequency of the suppressor with respect to the characteristic frequency (Costalupes *et al.*, 1987; Javel *et al.*, 1983; Delgutte, 1990; Ruggero *et al.*, 1992; Rhode and Cooper, 1996). This property of two-tone suppression will influence the responses of AN fibers to complex wide-band sounds. The present model includes this asymmetrical aspect of two-tone suppression as well as the compressive nonlinearity associated with the cochlear amplifier.

The model described here significantly extends a previous model developed by Carney (1993), which included compression and level-dependent bandwidths and phases, but not realistic two-tone suppression. The wide-band, feed-forward control path in the present model replaces the feedback control mechanism used in the previous model and is critical for including two-tone suppression. Wide-band suppression mechanisms superimposed on the more narrowly tuned excitatory process have previously been suggested as explaining some of the properties of two-tone suppression (Geisler and Sinex, 1980; Delgutte, 1990).

The model proposed here joins several other phenomenological models of basilar membrane and/or AN responses. This model focuses on the nonlinear response properties of auditory-nerve fibers described above, especially the level-dependent phase properties and two-tone suppression. Level-dependent phase properties of AN responses have not been a focus of other modeling studies, but several have addressed the problem of two-tone suppression and related nonlinear response properties.

Several modeling studies have explored combinations of linear filters and memoryless nonlinearities that provide phenomenological representations of responses at the level of the basilar membrane (without inclusion of models for the inner hair cells and IHC-AN synapse). Initial models of this type included the bandpass nonlinearity (BPNL) models of Pfeiffer (1970) and Duifhuis (1976). Goldstein (1990, 1995) extended this approach with a multiple bandpass nonlinear (MBPNL) model, which included two interacting paths, one with a low-pass filter followed by a memoryless nonlinearity, and one with a bandpass filter. Several nonlinear cochlear response properties can be explained by this model due to the level-dependent interaction of the two paths, which can be thought of as representing multiple modes of BM excitation (e.g., Lin and Guinan, 2000).

The MBPNL model describes level-dependent iso-reponse tuning curves that include ''tails,'' as well as several aspects of two-tone rate suppression, including the asymmetry of suppression for low-side versus high-side suppressors, synchrony capture by low-frequency tones, simple-tone interference, and the generation of combination tones (Goldstein, 1990, 1995; Lin and Goldstein, 1995). While there is some overlap between the phenomena described by the present model and by the MBPNL model, there are several important conceptual differences between the two modeling approaches. The MBPNL model consists of parallel pathways comprised of static filters that interact through memoryless nonlinearities, whereas the model presented here consists of a simple bandpass filter with time-varying gain and bandwidth. In addition, most of the simulations presented here include models for the IHC and the IHC-AN synapse; the goal of this model is to provide AN discharge patterns (as opposed to cochlear responses), and comparisons of model output are primarily made to AN response properties described in the literature. The detailed relationship between phases of BM and AN responses, which vary with stimulus frequency, characteristic frequency (CF, the frequency to which an AN fiber is most sensitive), and SPL (e.g., Ruggero and Rich, 1987; Narayan *et al.*, 1998; Cheatham and Dallos, 1999) are beyond the scope of this study.

The level-dependence of the phase of BM (e.g., Geisler and Rhode, 1982; Ruggero *et al.*, 1997), IHC (Cheatham and Dallos, 1998), and AN (e.g., Anderson *et al.*, 1971) responses to tones at frequencies above and below CF is a nonlinear response property that is potentially important for the encoding of complex sounds (e.g., Carney, 1994). This property cannot be described by the MBPNL model. The study presented here examines the relationship between level-dependent phase and two-tone suppression and illustrates that a single mechanism can be used to incorporate both properties in a phenomenological model. Note that the model presented here does not attempt to include all of the properties explained by the MBPNL and other models. In particular, tails of tuning curves and simple-tone interference, which can be explained by MBPNL models, are not addressed by this model. Also, this model does not include asymmetrical filter shapes, which are the focus of Irino and Patterson's (1997) auditory filter model that includes a level-dependent ''glide'' of the instantaneous frequency of AN impulse responses as a function of time. Actual BM and AN responses have glides that are level-independent (e.g., Recio *et al.*, 1996; de Boer and Nuttall, 1997; Carney *et al.*, 1999), and the direction of the glide varies with CF in AN responses (Carney *et al.*, 1999). Inclusion of this potentially important temporal response property into an AN model would be of interest for future studies.

Another feature of several AN models is the inclusion of high, medium, and low spontaneous-rate AN fibers (Liberman, 1978). Sachs and Abbas (1974) and Schoonhoven *et al.* (1998) investigated phenomenological models that explained rate-level functions for AN fibers with different spontaneous rates in terms of the relation between AN threshold and BM compression. Also, detailed models of the IHC-AN synapse (e.g., Schwid and Geisler, 1982; Meddis, 1986, 1988; Westerman and Smith, 1988; Geisler, 1990; Hewitt and Meddis,

1991; Lopez-Poveda *et al.*, 1998) provide descriptions of several features of AN rate-level functions. In the study presented here, results are limited to high spontaneous-rate AN fibers.

One benefit of the filterbank model developed here is that it allows the simulation of population responses of AN fibers to simple and complex sounds. Previous models have also been developed for this purpose, and these models share some of the properties of the present model. Jenison *et al.* (1991) developed a composite model for AN responses that included level-dependent peripheral filter bandwidths, which were based on filters derived from a database of AN rate-level functions. Deng and Geisler (1987) developed a composite model for AN responses based on a nonlinear cochlear model with longitudinal stiffness coupling. Giguere and Woodland (1994) proposed an analog/digital composite model that included the compressive nonlinearity. All of these models were tested primarily with speech stimuli, and showed several interesting features, such as synchrony capture by low-frequency formants. None of these models were tested closely using simple tones or pairs of tones to explore the details of their level-dependent phase properties or details of two-tone suppression.

The model described in the present study shares some general features with a recent model proposed by Robert and Eriksson (1999), which included nonlinear gain, bandwidth, and some aspects of two-tone suppression. However, the Robert and Eriksson (1999) model did not address several key response properties that are a focus of the present study. For example, their study did not include the temporal response properties of AN fibers, such as the dependence of synchrony on level and frequency, and the level-dependence of the phase of phase-locked responses. In addition, they did not address the asymmetry in suppression growth above and below CF. Their model involved a feedback control mechanism that combined control signals from neighboring fibers with different CFs to achieve an effectively wider-band control path, and thus wide-band two-tone suppression.

In the present study, the strategy is instead to use a wide-band feedforward path, which allows the properties of two-tone suppression to be included in a model of a single CF fiber (without having to simulate responses of the neighboring fibers). Furthermore, the level-dependent gain and bandwidth of the feedforward control path in the present model allow the asymmetry of two-tone suppression to be included. Because studies of information coding in the auditory system are still investigating the roles of temporal information and/or average discharge rate, this model was designed to simulate both aspects of the AN discharges with as much accuracy as possible, over wide ranges of CF and SPL.

This report presents the overall design and implementation of the model and shows responses of the model to a number of stimuli that have been used in physiological studies of AN fibers. The next section describes each stage of the model and its parameter values (either in equations or in a table), justification for parameter choices, and an explanation of the major effects of each parameter. Following the model description, response properties of the model are shown and discussed. Model responses are compared to several examples of AN responses from the literature; note that the parameters of the model were the same for all simulations. However, the levels of the stimuli tested were sometimes adjusted to accommodate differences in threshold between the model and a particular AN fiber. The model parameters are primarily based on the responses of AN fibers in cat; however, data from other species were used when necessary. The model presented here is focused on nonlinear tuning properties and is limited to high-spontaneous-rate AN fibers. Interactions between nonlinear aspects of basilar-membrane tuning and the properties of the IHC-AN synapse create different response properties for low- and medium-spontaneous-rate AN fibers (Sachs and Abbas, 1974). Future study in this series will focus on inclusion of more detail in the IHC-AN synapse, as well as the interaction of the properties of the synapse with the other nonlinear features of the present model, and will thus extend this model to include the other spontaneous-rate groups.

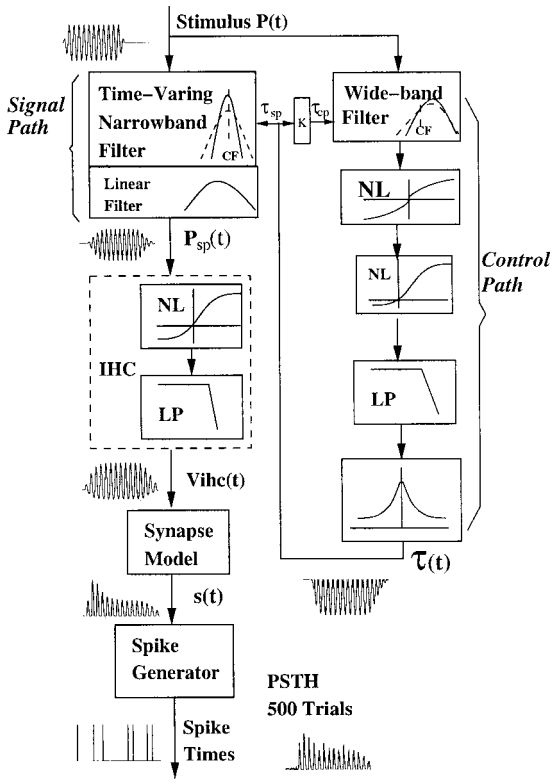

FIG. 1. Block diagram of the AN model. The waveforms that illustrate the output of each stage are the responses of a 500 Hz CF fiber to a 50 dB SPL pure tone at CF.

II. MODEL DESCRIPTION

A. Overview

The general scheme of the AN model implementation[1] is illustrated in Fig. 1. The input to the model is the instantaneous pressure waveform of the stimulus in Pascals. The effects of the external and middle ears are not considered here. The model includes properties described in recent physiological studies of the auditory system; however, it is a phenomenological model and the main effort is to simulate realistic level-dependent average-rate and temporal re-

sponses of AN fibers with the simplest possible model. To determine the model parameters, experimental data available in the literature were used whenever possible and reasonable assumptions were made when there were no data to support a particular parameter value. The selection of parameters and equations in the model was guided mainly by the response properties of the model rather than by the mechanisms of the actual physiological system. The two major parts of the nonlinear filtering section of the model are the *signal path* and the feedforward *control path* (Fig. 1).

The tuning of the signal path (corresponding roughly to tuning on the basilar membrane) is modeled by a cascade of a time-varying filter and a linear filter. The control path acts to regulate the tuning of the time-varying signal-path filter and is responsible for the compression and suppression effects observed in model AN responses. The bandpass filter in the control path has a broader bandwidth than the signal path to achieve two-tone suppression over a wide frequency range. A saturating nonlinearity followed by a low-pass filter in the control path determines the dynamic range and the dynamics of the compression and suppression. The control signal is then shifted and scaled to adjust the threshold and range of compression (each fiber is scaled based on its CF). The output of the signal-path filter is then passed through models for the IHC and IHC-AN synapse that represent corresponding processing stages in the cochlea. A nonhomogeneous Poisson-process model with refractory effects is used to generate the discharge times of the AN fiber. Brief descriptions and values for all model parameters are provided in Table I.

B. Signal-path filter

The signal-path filter represents the tuning properties of a specific location on the basilar membrane; the output of the signal-path filter provides the input to the IHC model. The signal path consists of a time-varying filter followed by a linear filter. The gain and bandwidth of the time-varying narrow-band filter are changed continuously as the control signal fluctuates, varying on a cycle-by-cycle basis with stimulus fluctuations below 800 Hz (limited by the low-pass filter in the control path). The signal-path time-varying filter is the source of the level-dependent-phase and the two-tone-suppression response nonlinearities illustrated in the figures below. The nonlinear filter also introduces asymmetry in the output signal, resulting in a dc component that varies across stimuli and sound levels. This dc component (which may or may not be biophysically appropriate) is difficult to accommodate using the simplified model stages that follow the nonlinear signal-path filter. Therefore, the final stage in the signal-path filter is a linear bandpass filter that eliminates the dc component of the response.

Both the time-varying nonlinear filter and the linear filter in the signal path were based on gammatone filters, which have been used in several studies to represent the impulse responses of AN fibers (Johannesma, 1972; de Boer, 1975; de Boer and de Jongh, 1978; de Boer and Kruidenier, 1990; Carney and Yin, 1988; Carney, 1993). The impulse response of the gamma-tone filter is given by

$$g(t) = u(t-\alpha)(t-\alpha)^{\gamma-1} e^{-(t-\alpha)/\tau} \cos[\omega_{\mathrm{CF}}(t-\alpha)] \quad (1)$$

where $u(\cdot)$ is the unit-step function, α is a delay added to the gammatone response, τ is the time constant, ω_{CF} is the radian frequency corresponding to the characteristic frequency (CF) of the model fiber, and γ is the order of the filter. This function has a simple expression in the frequency domain (Patterson *et al.*, 1988):

$$\begin{aligned} G(\omega) &= 0.5\tau^{\gamma}(\gamma-1)!\, e^{-j\omega\alpha}\left[\frac{1}{[1+j\tau(\omega-\omega_{\mathrm{CF}})]^{\gamma}}\right. \\ &\quad \left. + \frac{1}{[1+j\tau(\omega+\omega_{\mathrm{CF}})]^{\gamma}}\right] \\ &\cong \frac{\tau^{\gamma}(\gamma-1)!\, e^{-j\omega\alpha}}{2[1+j\tau\cdot(\omega-\omega_{\mathrm{CF}})]^{\gamma}}, \quad \omega_{\mathrm{CF}} \gg 0, \end{aligned} \quad (2)$$

where j is $\sqrt{-1}$.

The signal path consists of a nonlinear third-order gammatone filter followed by a linear first-order gammatone filter. The nonlinear filter is implemented by frequency shifting the input signal downward by CF, then using a cascade of three first-order low-pass filters, based on the strategy of Patterson *et al.* (1988). The low-pass filters were implemented digitally using the IIR bilinear transformation (Oppenheim and Schafer, 1975). The time delay α in the nonlinear filter is the additional delay that is required for a gammatone filter to represent the AN impulse response, including traveling-wave, acoustical, and synaptic delays (Carney and Yin, 1988; Shera and Guinan, 2000). The delay is a function of CF, estimated from fits of gammatone functions to measured reverse-correlation functions (Carney and Yin, 1988; Carney, 1993):

$$\alpha(\mathrm{CF}) = A_D e^{-x_{\mathrm{CF}}/A_L} - 2\pi/\omega_{\mathrm{CF}}, \quad (3)$$

where A_D and A_L are from Carney (1993) and x_{CF} is the distance (mm) from the apex of the basilar membrane from Liberman's (1982) frequency map for cat.

From Eq. (2) it is clear that both the gain and bandwidth of the filter are controlled by the time-varying time constant $\tau(t)$. The output of the control path specifies the time constant $\tau_{sp}(t)$ for each of the three first-order gammatone filters in the cascade that comprises the time-varying third-order filter in the signal path. The time constant $\tau_{sp}(t)$ varies over a range determined by τ_{narrow} (for sharp tuning at low SPL) and τ_{wide} (for broad tuning at high SPL), where τ_{narrow} is greater than τ_{wide}. The time-invariant time constant for the first-order linear gammatone filter in the signal path is set to τ_{wide} and the gain of this filter is set to 0 dB at CF. The values of τ_{narrow} and τ_{wide} are determined by the tuning properties of AN fibers. A linear fit of measured values of Q_{10} (the ratio between CF and bandwidth measured 10 dB above the fiber threshold) for cat AN fibers (Miller *et al.*, 1997) determines the value of τ_{narrow}:

$$\tau_{\mathrm{narrow}} = \frac{2Q_{10}}{2\pi\mathrm{CF}}, \quad (4)$$

where the $Q10$ data is fit by

$$\log_{10}(Q_{10}) = 0.4708\log_{10}(\mathrm{CF}/1000) + 0.4664. \quad (5)$$

TABLE I. Description of the parameters used in the AN model. The desired values of PST histogram characteristics are used to derive parameter values for Westerman and Smith's (1988) three-store diffusion model (see the Appendix). The resulting values of these characteristics for the model response are not the same as these input parameter values due to the effects of refractoriness. For example, the spontaneous rate of the model fiber response is approximately 45 spikes/s, rather than the 50 spikes/s indicated in the table below (see Fig. 7).

Parameters	Description	Values
Basilar membrane tuning filter and control path		
ω_{CF}	characteristic frequency of the fiber (rad/s)	
α	delay of the onset tone responses for cat (s)	See Eq. (3)
A_D	coefficient for traveling wave delay (ms)	8.13
A_L	length constant for traveling wave delay (nm)	6.49
x_{CF}	distance from apex of basilar membrane (mm)	
$\tau(t)$	output of the control path	
τ_{narrow}	estimated time constant at low sound level	See Eq. (4)
τ_{wide}	estimated time constant at high sound level	See Eq. (6)
γ_{cp}	order of the wide bandpass filter in control path	3
ω_{cp}	center frequency of the wide bandpass filter	1.2 mm basal to fiber CF
K	ratio of time constant in control path to that in signal path	$0.2+0.8\ \tau_{\mathrm{wide}}/\tau_{\mathrm{narrow}}$
A_{cp}	parameter in logarithmic nonlinearity	970
B_{cp}	parameter in logarithmic nonlinearity	2.75
C_{cp}	parameter in logarithmic nonlinearity	0.69
$x0_{cp}$	parameter in Boltzman function	7.6
$s0_{cp}$	parameter in Boltzman function	12
$x1_{cp}$	parameter in Boltzman function	5
$s1_{cp}$	parameter in Boltzman function	5
shift_{cp}	parameter in Boltzman function	0.125
cut_{cp}	cutoff frequency of control-path low-pass filter (Hz)	800
k_{cp}	order of control-path low-pass filter	3
dc	estimated dc shift of CP low-pass filter output at high level	0.37
R_0	ratio of τ_{LB} (lower bound of τ_{SP}) to τ_{narrow} [see Eq. (13)]	0.05
Inner hair cell model		
A_{ihc0}	scalar in IHC nonlinear function [see Eq. (16)]	0.1
B_{ihc}	parameter in IHC nonlinear function [see Eq. (15)]	2000
C_{ihc}	parameter in IHC nonlinear function [see Eq. (16)]	1.74
D_{ihc}	parameter in IHC nonlinear function [see Eq. (16)]	6.87*e*-9
cut_{ihc}	cutoff frequency of IHC low-pass filter (Hz)	3800
k_{ihc}	order of IHC low-pass filter	7
p_1	parameter in V_{ihc} rectifying function	0.0143
p_2	parameter in V_{ihc} rectifying function	See Eq. (18)
Synapse		
spont	spontaneous rate of fiber (spikes/s)	50
A_{SS}	steady state rate (spikes/s)	350
τ_{ST}	short-term time constant (ms)	60
τ_R	rapid time constant (ms)	2
$A_{R/ST}$	rapid response amplitude to short-term response amplitude ratio	6
PTS	peak to steady state ratio	8.6
$P_{I\ \max}$	permeability at high sound level	0.6
Spike generator and refractoriness		
$c0$	parameter for relative refractoriness	0.5
$c1$	parameter for relative refractoriness	0.5
$s0$	parameter for relative refractoriness (ms)	1.0
$s1$	parameter for relative refractoriness (ms)	12.5
R_A	absolute refractory period (ms)	0.75

While τ_{narrow} is based on physiological data in the literature and is the main parameter for the sharp low-level tuning of the signal-path filter, the actual tuning properties of the complete model output are affected by the compressive nonlinearity of the model. The parameter τ_{wide} is chosen based on the desired filter gain at high levels. The difference between τ_{wide} and τ_{narrow} is directly related to the gain of the cochlear amplifier at a given CF:

$$\tau_{\mathrm{wide}}=\tau_{\mathrm{narrow}}10^{-\mathrm{gain(CF)}/60}, \tag{6}$$

based on the third-order nonlinear filter.

The gain of the cochlear amplifier, or equivalently the amount of compression in the model, is a simple function of CF and is limited between 15 dB (at low CFs) and 70 dB (at high CFs) as follows:

$$\text{gain(CF)} = \max\{15, \min[70,\ 20 + 42\log_{10}(\text{CF}/1000)]\}. \quad (7)$$

The gain of the cochlear amplifier, or the amount of compression, has not been well characterized at many CFs in cat. The function above was chosen based on a maximum gain of 70 dB for high-CFs (Ruggero *et al.*, 1997; Nuttall and Dolan, 1996) and a minimum gain of around 15 dB at low CFs (Cooper and Rhode, 1996, 1997) observed in other mammalian species, with a smooth transition between low and high CFs, as observed psychophysically in humans (Hicks and Bacon, 1999). This gain function could be easily modified when data are obtained from cat; however, the present implementation represents the generally accepted concept that there is stronger compression at high CFs than at low CFs. For model responses to pure tones at stimulus frequencies more than an octave away from CF, there was not much change in gain as a function of stimulus level [see Eq. (2)], which is consistent with the data of Ruggero *et al.* (1997).

C. Wide-band feedforward control path

The function of the control path is to provide a time-varying signal $\tau_{sp}(t)$ to the signal-path filter such that several level-dependent response properties can be replicated by the signal-path filter. The control path is designed to reflect the active process corresponding to the local CF place as well as to the neighboring CFs. The control path consists of (a) a time-varying bandpass filter with a broader bandwidth than the signal-path filter; (b) a symmetrical nonlinear function to compress the dynamic range of the control signal; (c) a nonlinear function followed by a low-pass filter to control the dynamic range and dynamics of compression; and (d) a nonlinear function to adjust the total strength of compression.

The wide-band control filter is a third-order gammatone filter with its center frequency shifted 1.2 mm basal to the fiber CF along the basilar membrane (i.e., higher in frequency than CF). The size of the shift of the wide-band filter and the order of the filter were based on the shape of AN suppression tuning curves in the literature (e.g., Sachs and Kiang, 1968; Arthur *et al.*, 1971; Delgutte, 1990). The bandwidth of the nonlinear wide-band control-path filter is varied by $\tau_{cp}(t)$, which is a scaled version of $\tau_{sp}(t)$, the signal that controls the bandwidth of the nonlinear filter in the signal path. The scaling of $\tau_{sp}(t)$ by the factor K (<1, see Table I to create $\tau_{cp}(t)$ (Fig. 1) guarantees that the control-path filter has a wider bandwidth than the time-varying signal-path filter, and that the bandwidth ratio is constant. The gain of the wide-band control-path filter is normalized to 0 dB at the signal-path CF instead of at the center frequency of the control-path filter. As a result, the level-dependence of the gain of the control-path filter differs for frequencies above and below CF. This asymmetry is the key to producing the different properties of low-side and high-side suppression in the present model.

The analytical description of the control-path filter is given by the equation:

$$G_{cp}(\omega) \cong \{\text{gain}_{cp}(t)/[1 + jK\tau_{sp}(t)(\omega - \omega_{cp})]\}^{\gamma_{cp}} e^{-j\omega\alpha}, \quad (8)$$

where

$$\text{gain}_{cp}(t) = \sqrt{1 + [K\tau_{sp}(\omega_{\text{CF}} - \omega_{cp})]^2}, \quad (9)$$

j is $\sqrt{-1}$, and ω_{CF} is the radian frequency corresponding to the fiber's CF. The center frequency of the wideband control-path filter, ω_{cp} was computed using Liberman's (1982) frequency map based on the 1.2 mm basal shift from CF. The parameter $\text{gain}_{cp}(t)$ is calculated for every time step of the simulation to normalize the gain of the control-path filter to 0 dB at CF.

Experimental data show that the cochlear response is linear at low sound levels and becomes compressive at medium and high levels (Ruggero *et al.*, 1997). The slope of the compression has been shown to be as low as 0.2 dB/dB in the range of 40–80 dB SPL. Two different saturating nonlinear functions are used in the control path to implement this compression. A symmetrical logarithmic function

$$V[x(t)] = \text{sgn}[x(t)] B_{cp} \log(1 + A_{cp}|x(t)|^{C_{cp}}), \quad (10)$$

where $x(t)$ represents the output signal of the control-path filter; A_{cp}, B_{cp}, and C_{cp} are parameters which determine the (compressed) dynamic range of the signal before the second nonlinearity. The second function, an asymmetrical saturating nonlinearity, is a second-order Boltzmann function with an asymmetry of 7:1 (Mountain and Hubbard, 1996), given as

$$\text{out}(V) = \frac{1}{1 - \text{shift}_{cp}} \times \left\{ \frac{1}{1 + e^{-(V - x0_{cp})/s0_{cp}}\left(1 + e^{-(V - x1_{cp})/s1_{cp}}\right)} - \text{shift}_{cp} \right\}, \quad (11)$$

where $x0_{cp}$, $s0_{cp}$, $x1_{cp}$, and $s1_{cp}$ are parameters, and

$$\text{shift}_{cp} = \frac{1}{1 + e^{x0_{cp}/s0_{cp}}\left(1 + e^{x1_{cp}/s1_{cp}}\right)}. \quad (12)$$

The parameters in the two nonlinear functions above were adjusted by comparing compression-versus-level curves for the signal-path filter to physiological BM responses described in the literature (e.g., Ruggero *et al.*, 1997). The parameter A_{cp} determines the level at which the signal-path filter became nonlinear. Together with the parameters in the Boltzmann function, B_{cp} determines the level at which the signal-path filter became less compressive again. The parameter shift_{cp} guarantees that the nonlinear function passes through the origin. The parameter values are reported in Table I; these parameter values are invariant as a function of CF.

The two nonlinear functions are followed by a third-order low-pass filter. The cutoff frequency of the low-pass filter in the control path is set to 800 Hz. This cutoff frequency was chosen to produce an approximately 0.2 ms time constant for the onset of the compressive nonlinearity, consistent with the time course of compression estimated from click responses of the basilar membrane (see Fig. 8 in Recio *et al.*, 1998).[2]

The last stage of the control path is a nonlinear function that converts the output of the low-pass filter, $V_{LP}(t)$, to the time-varying time constant of the signal-path filter (Fig. 1):

$$\tau_{sp}(t)=\tau_{\text{narrow}}\left[R_0+(1-R_0)\left(\frac{\tau_{\text{wide}}/\tau_{\text{narrow}}-R_0}{1-R_0}\right)^{|V_{LP}(t)|/dc}\right]. \quad (13)$$

$\tau_{sp}(t)$ varies continuously between a maximal value of τ_{narrow} (which corresponds to a long time-constant, for a narrowly tuned filter) and an asymptotic lower bound, τ_{LB}. The value of R_0 is determined by the ratio $\tau_{LB}/\tau_{\text{narrow}}$. The parameter dc is an estimate of the dc component of the control-path output at high levels (i.e., a measure of the asymmetry of the control-path nonlinearities). The nonlinear function in Eq. (13) varies the dc value of $\tau_{sp}(t)$ from τ_{narrow} at low levels to τ_{wide} at high levels [see Eq. (6) for τ_{wide}]. The even function described in Eq. (13) causes the signal-path filter to be compressive for both the positive and negative parts of the instantaneous stimulus pressure for low frequency stimuli (Cooper, 1996). Note that the nonlinear filters in both the signal path and the control path are controlled by varying the filter time constants and associated gains: thus these filters are inherently stable (as long as positive time-constants and finite gains are specified). The time-varying time constant for the control path is simply a scaled version of the time constant for the signal path:

$$\tau_{cp}(t)=K\tau_{sp}(t) \quad \text{where} \quad K=0.2+0.8\frac{\tau_{\text{wide}}(\text{CF})}{\tau_{\text{narrow}}(\text{CF})}. \quad (14)$$

D. IHC-AN synapse

Physiological studies have shown that the IHCs transduce the mechanical responses of the basilar membrane to an electrical potential that results in the release of neurotransmitter at the synapse between the IHC and the AN fiber to generate action potentials in the AN fiber. Many studies have explored IHC potential changes in response to different stimuli. It is widely agreed that the synchrony coefficient of fibers responding to tones is affected by the ratio of the ac and dc components of the IHC response (e.g., Dallos, 1985; Palmer and Russell, 1986). This finding is the guideline for the analytical description of the present IHC model. The nonlinear function in the IHC model is a logarithmic compressive function

$$V_{\text{ihc}}(t)=A_{\text{ihc}}[P_{sp}(t)]\log(1+B_{\text{ihc}}|P_{sp}(t)|), \quad (15)$$

where $P_{sp}(t)$ is the output of the signal-path filter (Fig. 1). The function $A_{\text{ihc}}[P_{sp}(t)]$ and the parameter B_{ihc} were adjusted to achieve the appropriate IHC response properties, as follows: The asymmetry of the nonlinear function for $A_{\text{ihc}}[P_{sp}(t)]$, given by

$$A_{\text{ihc}}[P_{sp}(t)]=\begin{cases}A_{\text{ihc0}} & \text{for } P_{sp}(t)>0\\ -\dfrac{|P_{sp}(t)|^{C_{\text{ihc}}}+D_{\text{ihc}}}{3^*|P_{sp}(t)|^{C_{\text{ihc}}}+D_{\text{ihc}}}A_{\text{ihc0}}, & \text{for } P_{sp}(t)<0\end{cases} \quad (16)$$

changes smoothly as a function of the level of its input, $P_{sp}(t)$, from 1:1 to 3:1, such that at low sound levels, the dc response increases with a slope of 2 dB/dB compared with the 1 dB/dB slope of the ac response (Dallos, 1985). A_{ihc0} is a scalar, and the values of B_{ihc}, C_{ihc}, and D_{ihc} are constants that determine the SPLs of the inflection in the ac and dc components of the nonlinear function (see Table I). Note that these parameters are invariant with CF. This function for $A_{\text{ihc}}[P_{sp}(t)]$ guarantees the appropriate relationship between ac and dc response components, as opposed to a hyperbolic tangent (e.g., Carney, 1993) or Boltzman function, and was thus critical for obtaining realistic synchrony-versus-level responses for pure tones across a wide range of CFs (especially between 1 and 4 kHz).

The low-pass filter in the inner hair cell is a seventh-order filter with a cutoff frequency of 3800 Hz. This cutoff frequency was chosen to match the maximum sync coefficient versus CF for the model to data from cat (Johnson, 1980). The high order of the low-pass filter likely represents not only the low-pass filtering properties of the IHC membrane but other low-pass mechanisms such as the calcium-related synaptic processes (Weiss and Rose, 1988).

The nonlinear IHC-AN synapse also affects the characteristics of the AN fiber discharge patterns. A simplified implementation of a previous time-varying three-store diffusion model (Westerman and Smith, 1988; Carney, 1993) was used in the present model. The parameters in the current model were determined according to the equations in the Appendix of Westerman and Smith (1988) based on desired characteristics of post-stimulus-time (PST) histograms for tones (see the Appendix). The values of parameters used in the model are provided in Table I. A detailed description and discussion of the synapse parameters and their effects on the PST histograms as a function of spontaneous rate will be discussed in another paper. The results presented here are limited to high-spontaneous-rate model fibers, and thus depend less strongly on the details of the synapse model.

The immediate permeability $P_I(t)$ is a soft rectifying function of the model inner-hair-cell response, V_{ihc} (Fig. 1), described as

$$P_I(t)=p_1\log(1+e^{p_2V_{\text{ihc}}(t)}), \quad (17)$$

where p_1 determines the immediate permeability at rest and the spontaneous rate of the model fiber. The parameter p_2 is given by

$$p_2=\begin{cases}1165 & \text{for CF}<685\ \text{Hz}\\ -5430+1010\log(\text{CF}) & \text{for CF}>685\ \text{Hz}\end{cases} \quad (18)$$

and determines the slope of the relationship between P_I and V_{ihc}. Therefore p_2 affects the threshold of the model fiber. The CF-dependence of p_2 in Eq. (18) adjusts the thresholds of model fibers at CF to be approximately 0 dB for all CFs. The numerical expressions in Eqs. (17) and (18) (and Table I for p_1) were derived from basic parameters related to the IHC-Synapse model (see the Appendix for details). The effects of the external and middle ears on the threshold of AN fibers can be included in future models by appropriately attenuating the input to the model as a function of frequency, referenced to the 0 dB baseline threshold in the present model. The output of the diffusion model is the time-varying discharge rate $s(t)$ prior to the inclusion of refractory effects,

where $s(t)=P_I(t)C_I(t)$. For further details of the IHC-AN synapse model, see the Appendix; also see the appendices of Westerman and Smith (1988) and Carney (1993).

E. Discharge generator

The model discharge times are produced by a renewal process that simulates a nonhomogeneous Poisson process driven by the synapse output $s(t)$ and modified to include refractory effects (Carney, 1993). The time-varying arrival rate of the Poisson process is described as

$$R(t)=s(t)[1-H(t)]. \tag{19}$$

The discharge-history effect, $H(t)$, was determined by a sum of two exponentials (Westerman and Smith, 1985):

$$H(t)=\begin{cases} c_0 e^{-(t-t_1-R_A)/s_0}+c_1 e^{-(t-t_1-R_A)/s_1} \\ \quad \text{for } (t-t_1)\geq R_A \\ 1.0 \quad \text{for } (t-t_1)<R_A \end{cases}, \tag{20}$$

where t_1 is the time of the preceding discharge, and c_0, c_1, s_0, s_1 are parameters (Table I). Discharges are not allowed to occur during the absolute refractory time R_A, and $H(t)$ varies continuously from 1 to 0 as the interval from the previous discharge increases beyond R_A. The statistics of the discharge are affected by refractoriness (Teich and Lachs, 1979), and the parameters in the expression for $H(t)$ (Table I) were adjusted to match the statistical properties of the responses (mean and variance of discharge rate) to published data (Young and Barta, 1986; Winter and Palmer, 1991).

III. RESULTS

A. Responses to pure tones

Figure 2 illustrates an overview of the responses of several model stages for three fibers tuned to different frequencies in response to 60 dB SPL pure tones at CF. The magnitude of the signal-path filter output $P_{sp}(t)$ decreases as the fiber's CF increases due to the larger compression at high CFs. The control signal $\tau(t)$, which varies the gain and bandwidth of the signal-path filter, varies on a cycle-by-cycle basis with the stimulus at low frequencies. At higher frequencies, the control signal becomes increasingly dominated by dc energy. Also, the IHC voltage $V_{\text{ihc}}(t)$ changes on a cycle-by-cycle basis at low frequencies, but is dominated by a dc bias for responses to pure tones at high frequencies. The adaptation in the diffusion model shapes the onset response of the fiber in the synapse output $s(t)$.

Threshold tuning curves are shown in Fig. 3(a) using the paradigm of Liberman (1978). The thresholds at CF are around 0 dB; these thresholds can be adjusted by adding a middle-ear model to simulate the changes in threshold as a function of frequency that contribute to the audiogram. The model's Q_{10} bandwidths [Fig. 3(b)] are comparable to Q_{10} data for normal cats from Miller *et al.* (1997). The high-CF fibers respond at low frequencies, despite the lack of an explicit ''tail'' (Kiang and Moxon, 1974; Kiang, 1975; Liberman, 1978; Narayan *et al.*, 1998) mechanism included in this model. This low-frequency response is due to distortion introduced by the nonlinear filter in the signal path. The low-frequency portion of the tuning curve for high-CF model fibers is strongly influenced by the cutoff frequency of the low-pass filter in the control path, which influences the dynamics of the nonlinear variation in tuning and thus the degree of distortion. The details of the low-frequency response (tail) of high-CF fibers were not a focus of this study.

The response to a CF tone grows at a rate less than 1 dB/1 dB due to basilar membrane compression. It has been reported by several authors (e.g., Ruggero *et al.*, 1997; Rhode and Cooper, 1996) that the basilar membrane responds linearly at low levels and is most compressive between 40 and 80 dB SPL. The growth rate for high-CF fibers can be as low as 0.2 dB/dB (Ruggero *et al.*, 1997). The compression gain (the gain difference between low levels and high levels) varies from approximately 10 dB to 70 dB as the CF of the fibers increases (Nuttall and Dolan, 1996; Cooper and Rhode, 1996, 1997; Ruggero *et al.*, 1997). The response magnitude (ac RMS) of the signal-path filter output as a function of CF-tone level is illustrated in Fig. 4(a). As the stimulus level increases, the average value of the control signal is decreases as the system changes from linear to compressive. At high levels, the model response is less compressive due to the saturation of the control path. The results of the model are similar to the nonlinear response properties described by Rhode and Cooper (1996) and Ruggero *et al.* (1997), except perhaps at levels above 80 dB SPL, where the most sensitive cochleae appear to have basilar-membrane responses that remain compressive at very high levels (Ruggero *et al.*, 1997). The amount of compression in the model as a function of CF is illustrated in Fig. 4(b).

As the level of the input tone is changed, the fiber response properties, such as average rate, synchrony, and PST-histogram shape, also change. The phases of the temporal AN responses are affected by continuous changes in the phase versus frequency properties of the signal-path filter; the phase properties of the signal-path filter are time-variant, as they are affected by the control-path signal. As the bandwidth of the signal-path filter changes, its phase properties also change. The temporal response properties are also affected by the low-pass filter in the IHC model, which limits the phase-locking of the response at high frequencies (and introduces a time-invariant phase shift). The diffusion model of the IHC-AN synapse also has some influence on temporal response properties, for example, interval statistics are influenced by the adaptation and refractory properties of the synapse model.

It is believed that depolarizing voltage responses of the IHC determine the detailed firing patterns in AN fibers. The neural synchrony of AN fibers especially depends on the ratio between the ac and dc components of the IHC receptor potential (Dallos, 1985; Palmer and Russell, 1986; Cheatham and Dallos, 1993). The ac and dc responses for model fibers at two CFs are shown in Fig. 5. For the fiber with a CF of 1 kHz, the ac potential always dominates the output of the IHC, resulting in a high synchronization coefficient. For high-CF fibers, the dc potential dominates the IHC output, and the synchronization coefficient is lower. At low levels, the dc response in the model increases at a rate of 2 dB/dB, and the ac response increases at a rate of 1 dB/dB, as re-

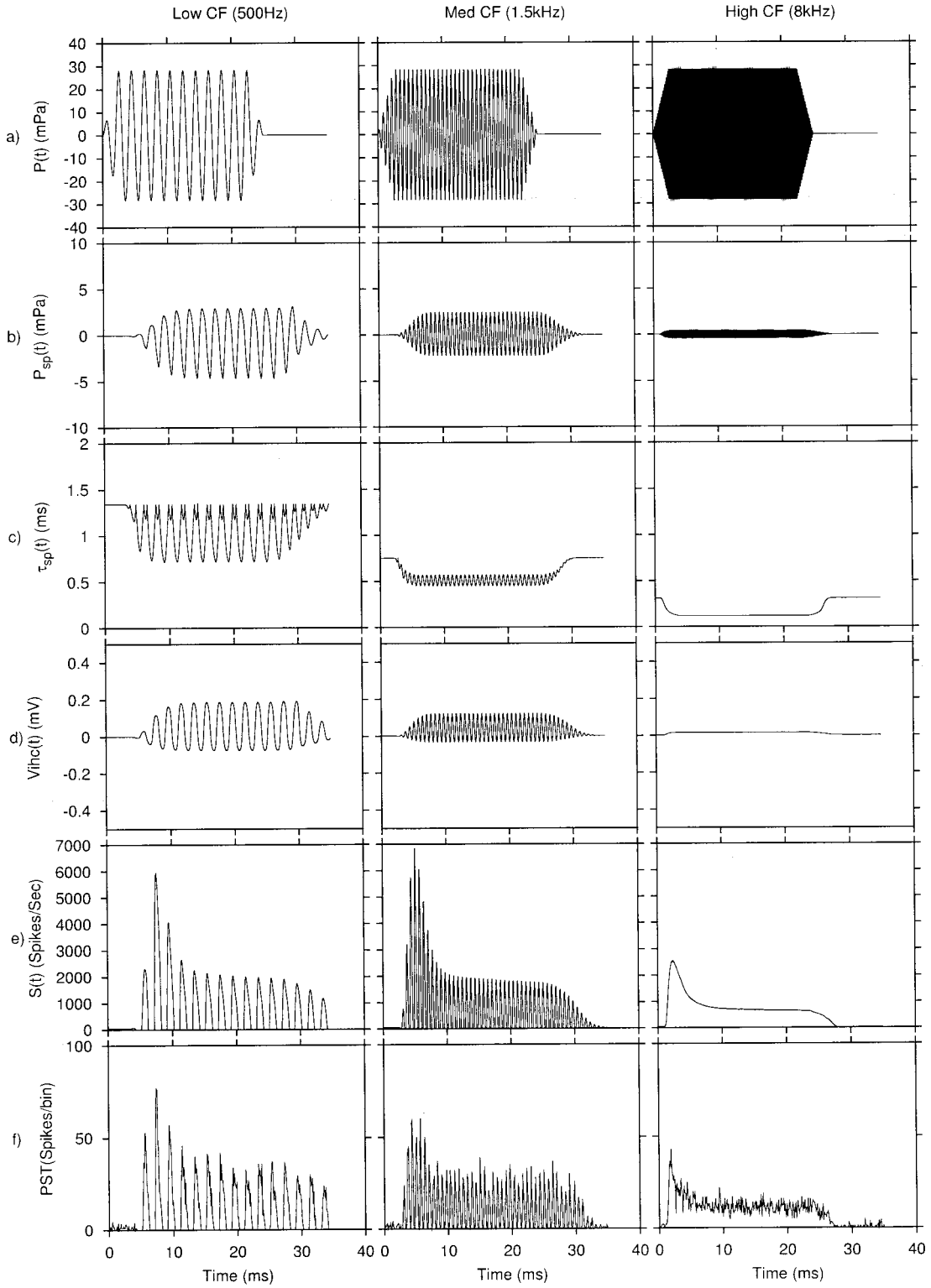

FIG. 2. Responses of several model stages to a CF tone for different model-fiber CFs. The stimulus was a 25 ms duration tone burst with a 2.5 ms rise/fall time and was presented at 60 dB SPL. The waveforms shown (see Fig. 1) are (a) $P(t)$, stimulus, (b) $P_{SP}(t)$, signal-path filter output, (c) $\tau(t)$ [or $\tau_{sp}(t)$], control signal, (d) $V_{IHC}(t)$, IHC response, (e) $S(t)$, synapse output, and (f) PST histogram based on 500 presentations and 0.1 ms bin size.

ported in the literature (Dallos, 1985). If a transition exists from an ac-dominated output to a dc-dominated output within the fiber's dynamic range, then experimental data would be expected to show dramatic nonmonotonic changes in the neural synchrony coefficient as a function of sound level, especially for mid-frequency CFs (1–4 kHz). This phenomenon is not found in experimental responses (Joris, 1999), and the model for the IHC was designed to avoid strongly nonmonotonic synchrony-level functions by using the asymmetrical function in Eq. (14).

Figure 6(a) shows the ac and dc responses of the IHC stage for an 800 Hz fiber in response to frequencies below,

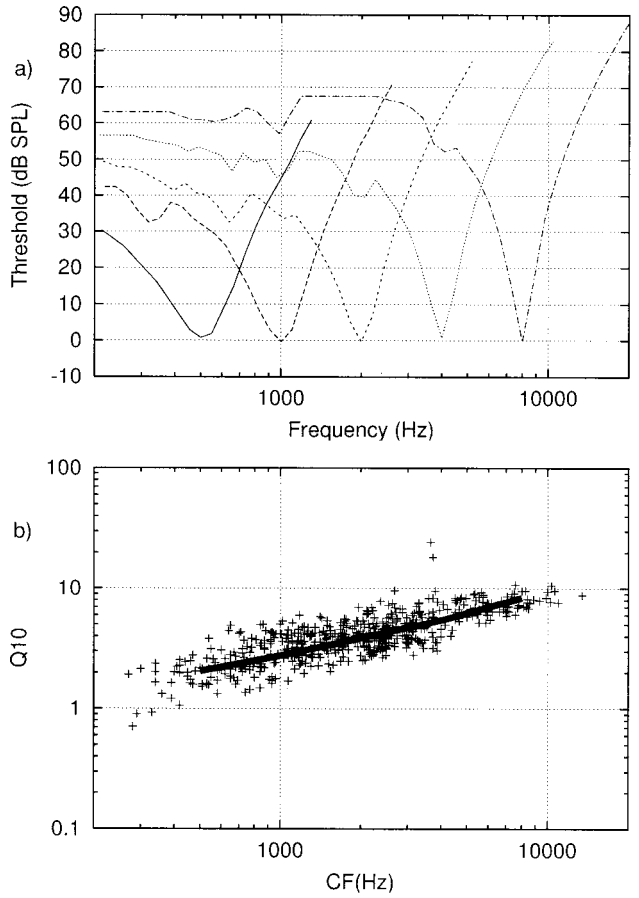

FIG. 3. (a) Threshold tuning curves for fibers with different CFs. The tuning threshold was defined as the level that results in a response 10 spikes/s greater than the spontaneous rate (200 repetitions of each stimulus). The stimulus is a 50 ms tone burst with a 2.5 ms rise/fall time (Liberman, 1978). Differences in discharge rates were counted between the 50 ms tone burst interval with 1.25 ms delay and the subsequent 50 ms silent interval. (b) Q_{10} measured from the tuning curve of model fibers (solid line) compared with the data (crosses) from Miller *et al.* (1997, Fig. 3). A linear fit of these data was used to determine the bandwidth of the signal-path filter at low SPLs. Q_{10} was then recomputed from the simulated tuning curves of the complete nonlinear model across a range of CFs to validate the model tuning.

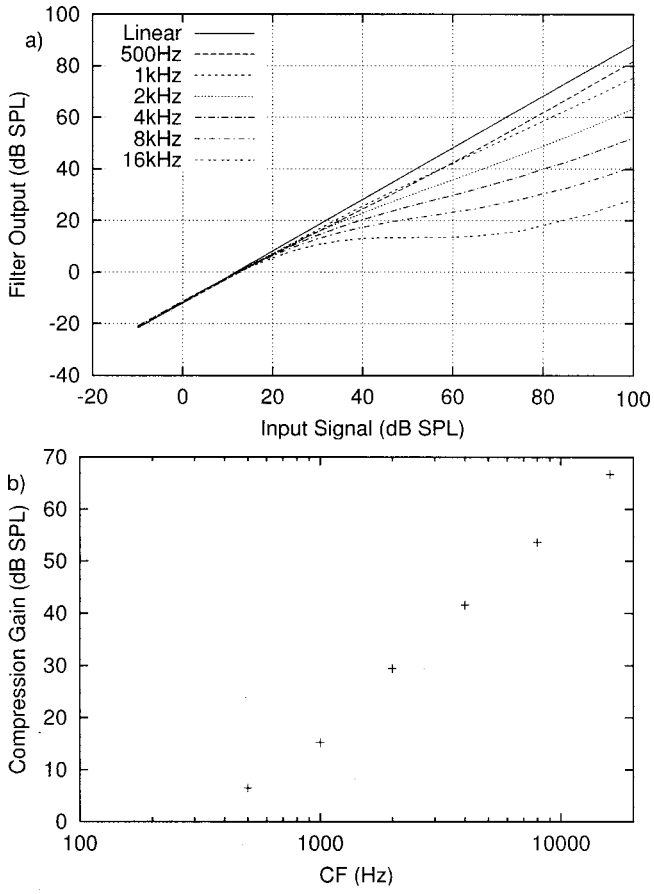

FIG. 4. Compressive nonlinearity of the signal-path filter output in response to CF tones for different CFs. (a) rms of the ac component (based on the peak-to-peak amplitude of the sinusoidal steady-state response) of the filter output as a function of stimulus intensity. The rms was computed from 10 cycles of the stimulus starting 40 ms after the onset of the stimulus. The solid line is the output of a linear filter. (b) Compression gain (the reduction in gain due to the compressive nonlinearity) for model fibers at different CFs. The compression gain was calculated as the difference of the gain of the responses to CF tones at 0 dB SPL and 120 dB SPL (Rhode and Cooper, 1996; Ruggero *et al.*, 1997).

at, and above CF. For comparison, Fig. 6(b) shows an example of ac and dc components of responses recorded from an IHC (Dallos, 1985). The model responses [Fig. 6(a)] to tones at frequencies below, at, and above CF are generally similar to the data, however, they do not saturate as completely as those shown in the examples from Dallos [Fig. 6(b)]. Other reports of IHC responses indicate that these cells may not completely saturate (e.g., Russell *et al.*, 1986), and recent models derived to fit IHC responses have incomplete saturation (e.g., Zagaeski *et al.*, 1994; Mountain and Hubbard, 1996). For example, the dotted curve in Fig. 6(a) shows the fit used by Zagaeski *et al.* (1994) to the dc component of IHC responses to tones well below CF. The relatively large dynamic range of the IHC response in the model is important in order to support the wide dynamic range of low-spontaneous-rate fibers, which will be pursued in future extensions of this model.

Figure 7 illustrates average discharge rate versus level and synchronization coefficient versus level functions in response to pure-tone stimuli at CF for fibers with CFs of 1 kHz and 4 kHz. The simulations presented in this study are limited to high-spontaneous-rate fibers; both fibers in Fig. 7 have spontaneous rates of about 45 sp/se. The sustained rate has a dynamic range of 40 dB and the onset rate has a wider dynamic range (Smith, 1988). The synchronization coefficient reaches its maximum at about 10 dB above threshold and then drops slightly as level increases, similar to AN-fiber responses (Johnson, 1980).

The increased dynamic range of the onset rate is a result of the adaptation included in the IHC-AN synapse model. This adaptation can also be illustrated by PST histograms of responses to tones (Fig. 8). The shape of the PST histogram changes as SPL is increased. The peak-to-sustained discharge rate increases with SPL, and the latency of the response decreases by integral multiples of 1/CF (Kiang *et al.*, 1965; Carney, 1993).

Rate and phase responses to pure tones at frequencies away from CF provide more information about the nonlinear

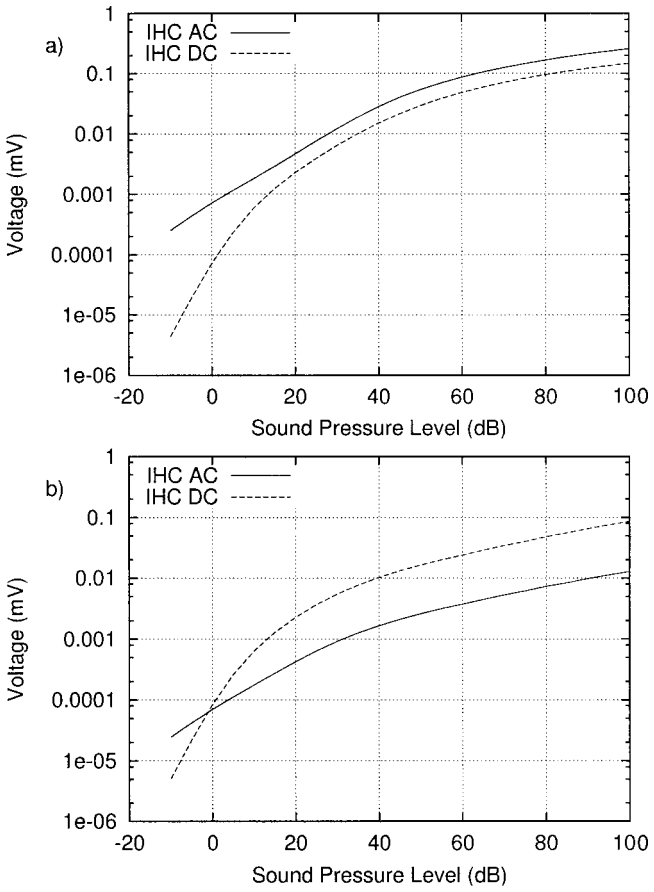

FIG. 5. IHC responses to pure tones at CF versus stimulus intensity for model fibers with CFs of (a) 1 kHz and (b) 4 kHz. The responses were measured over 10 cycles of the stimulus beginning 40 ms after the onset of the stimulus. The ac and dc components of the responses increase at different rates at low levels, and the dc component dominates the output as the CF of the fibers increases (Dallos, 1985).

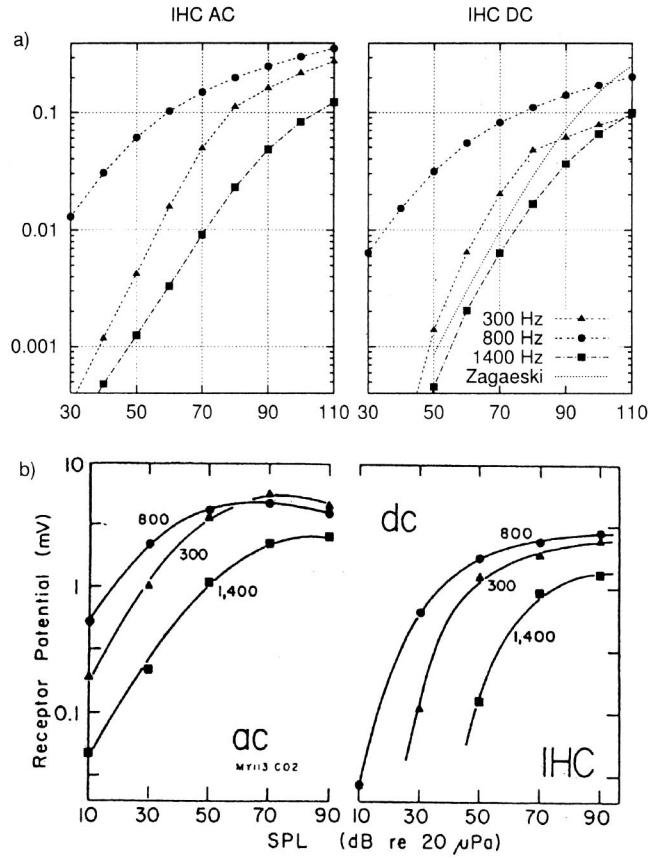

FIG. 6. ac and dc response components of (a) model IHC and (b) actual IHC responses (Dallos, 1985; with permission). Both model and actual IHCs have a CF of 800 Hz, responses to tones at 300, 800, and 1400 Hz are shown. The dynamic range of the model and actual responses are similar, although the threshold of the actual IHC in this example is lower than that of the model. The dotted line in the model dc response plot (upper right) is the fit of Zagaeski *et al.* (1994) to IHC responses to tones well below CF. Zagaeski *et al.*'s fit was shifted up to the normalized units of the IHC model (by setting Zagaeski *et al.*'s parameter $RP_{\max}$ to 0.6).

tuning of the model. Figure 9 illustrates the response area (responses to tones across a range of frequencies and levels) for an AN model fiber with CF of 2300 Hz, chosen for the purpose of comparison with the example shown from Anderson *et al.* (1971). Changes in rate as a function of level for frequencies above and below CF are illustrated in the upper panels. The response area (iso-level contours of discharge rate) spreads as the input level increases. A level-dependent shift in the peak frequency of the response area was not observed in the results due to the symmetry of the gammatone filter, which is a limitation of the model. Changes in the phase of phase-locked responses as a function of level, above and below CF, are illustrated in the lower panels. The phases are referenced to the response at 90 dB SPL, following Anderson *et al.*'s (1971) convention. Systematic level-dependent phase changes have been observed in basilar membrane motion (Ruggero *et al.*, 1997), in IHC responses (Cheatham and Dallos, 1993), and in AN fibers (Anderson *et al.*, 1971). The level-dependent change in phase of the phase-locked responses is consistent with the phase change expected due to broadening of the signal-path filter as level increases. The size of the phase change for low levels was comparable to the data from Anderson *et al.* (1971); maximum phase changes were approximately 0.5π.

Figure 10 illustrates level-dependent discharge rates and phases, across a range of stimulus frequencies, for a high-CF fiber. In this case, the phases were computed from the output of the signal-path filter and are compared to measurements of basilar-membrane phase from Ruggero *et al.* (1997). The phase change for high-CF model fibers was stronger than for the low-CF fiber because of the stronger compression at high-CFs [Fig. 4(b)]. Due to the rolloff in synchrony at high CFs (see below), it is difficult to compare the level-dependent phase at high CFs to AN responses. Illustration of the level-dependent phase based on the filter output also makes it clear that this phenomenon is a result of the nonlinear filter in the signal path. The IHC, synapse, and discharge generator models that follow the signal path do not introduce level-dependent phase shifts.

The maximum synchronization of responses to pure tones at CF as a function of CF is an important description of the temporal response of AN fibers. The synchronization coefficient was strongly influenced by the low-pass properties of the IHC model. Other factors, such as the low-pass properties of the synapse, also affect the synchronization of the AN fiber (Weiss and Rose, 1988). Figure 11 shows the maxi-

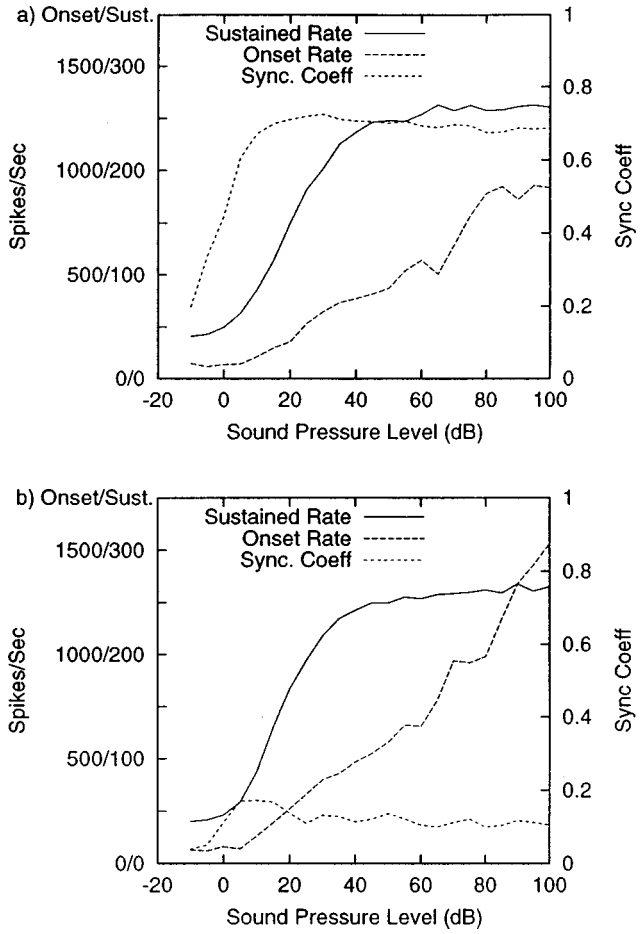

FIG. 7. Rate-Level and Sync-Level functions for model fibers with CFs of (a) 1 kHz and (b) 4 kHz. Sustained rate is calculated in the 10–45 ms response time window for 400 repetitions. Onset rate is the maximum discharge rate during the first 10 ms and was calculated using 0.5 ms bins (bin size is one stimulus cycle if the stimulus cycle is greater than 0.5 ms). The onset response in the figure is scaled (divided by 5.0) for better illustration. The discharges in the 10–45 ms time window were analyzed using a 32 bin period histogram from which the synchronization coefficient was then calculated (scale on right) (Johnson, 1980).

mum synchronization coefficient for the model and for data from cat (Johnson, 1980). The model synchronization coefficient is within the scattered data, but is slightly lower than the mean of the data. The parameters of the seventh-order low-pass filter and of the IHC-Synapse model were adjusted to achieve this representation of the rolloff in synchrony as a function of CF over the wide range of CFs modeled.

B. Responses to complex sounds

One goal of this study was to develop a model capable of simulating the responses of AN fibers to complex sounds. Interactions between different components of complex sounds have been studied for many years to gain a better understanding of these responses. Two-tone suppression is a nonlinear phenomenon of AN responses whereby the rate response to a pure tone at CF can be suppressed by a second tone (suppressor) (Nomoto *et al.*, 1964; Sachs and Kiang, 1968; Delgutte, 1990). More recent studies have reported two-tone suppression in the responses of IHCs and in cochlear mechanics (Cheatham and Dallos, 1989, 1990, 1992; Rhode, 1977; Ruggero *et al.*, 1992; Cooper and Rhode, 1996; Cooper, 1996). These observations have shown that the two-tone suppression nonlinearity originates in the mechanics of the cochlear partition (Ruggero *et al.*, 1992). Two-tone suppression is asymmetrical for low- and high-side suppressors, both in terms of the shape of the suppression threshold tuning curve and in the suppression growth rate for tones above and below CF (e.g., Arthur *et al.*, 1971; Prijs, 1989; Delgutte, 1990).

Figure 12 shows suppression tuning curves of two low-frequency model fibers with CFs at 1 kHz and 2 kHz. The asymmetry of the suppression-tuning threshold is due to the shift of the center frequency of the wide-band control-path filter with respect to the model fiber's CF. The asymmetry of the model suppression tuning curve is comparable to that reported in the literature across a range of CFs (e.g., Sachs and Kiang, 1968; Arthur *et al.*, 1971; Delgutte, 1990). Suppression was found even when the level of the suppressor was in the excitatory region of the tuning curve. This is because the CF tone level is set at a level which results in 2/3 of the maximum driven discharge rate (e.g., Delgutte, 1990), and the suppressor acts to suppress the response to the CF tone at this level. The relatively weak suppression for low-CF fibers, as compared to high-CF fibers (see below), especially for frequencies below CF, is due to the relatively

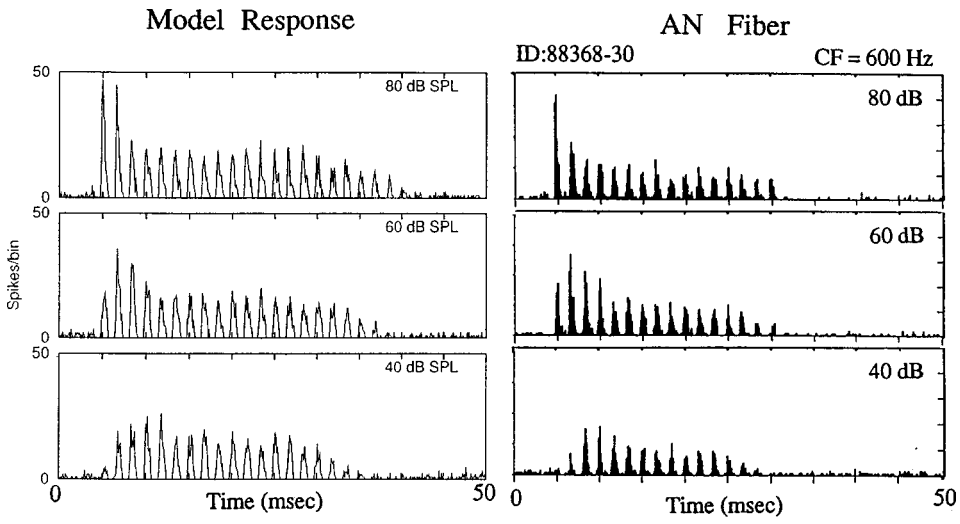

FIG. 8. PST histograms for (a) model and (b) actual AN fibers with CF equal to 600 Hz. Responses are to pure tones at CF at three different SPLs. The stimulus was 25 ms in duration and presented every 50 ms. The rise/fall time was 3.9 ms and the bin size was 0.1 ms. The PST histograms contain responses to 200 presentations at each SPL. The AN response was recorded as part of another study (Carney, 1990; see also Fig. 7, Carney, 1993).

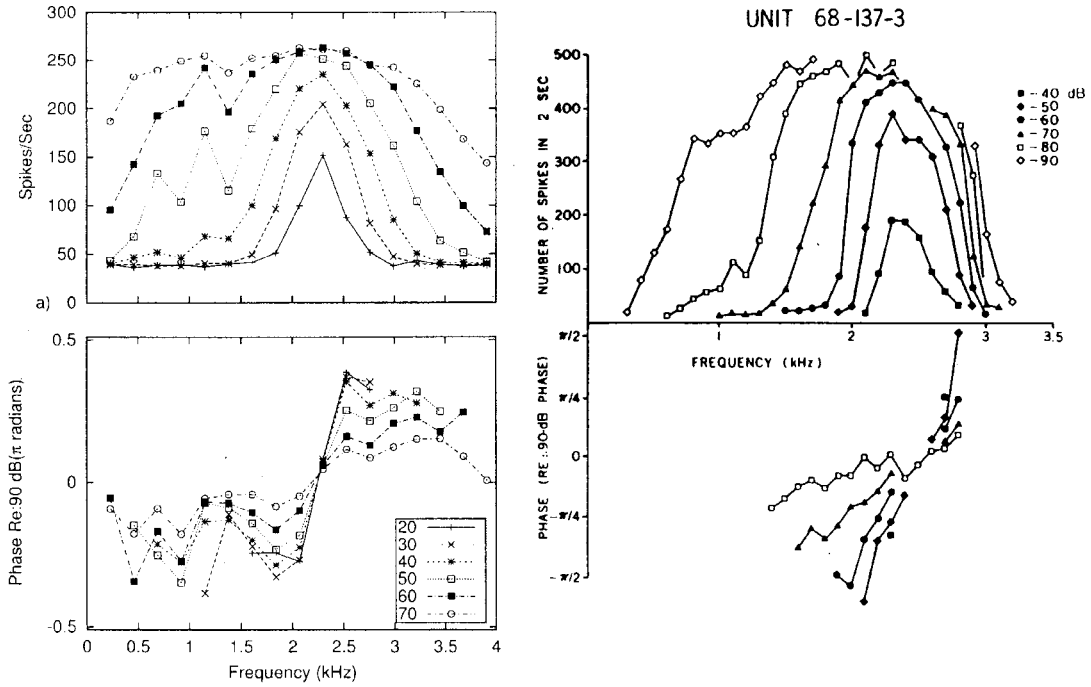

FIG. 9. Comparison of model and actual response areas. Left: Intensity-dependent discharge rate and phase responses for a model fiber with CF of 2300 kHz. Rates were computed from the sustained responses to 100 repetitions of a 50 ms tone burst. The phase for each response was referenced to the phase in response to that frequency at 90 dB SPL (e.g., Anderson *et al.*, 1971). Right: Rates and phases for the response area of an actual AN fiber with the same CF from Anderson *et al.* (1971, Fig. 8; with permission). The levels chosen for the model simulation (20–70 dB SPL) were selected to approximately match the levels, with respect to threshold, of Anderson *et al.*'s data set (i.e., note that the response of the model at 20 dB SPL is similar to the AN fiber's response at 40 dB).

low gain of the cochlear amplifier for low CFs [see Fig. 4(b)]. This pattern of suppression at low CFs is consistent with physiological data (Delgutte, 1990).

The upper panels of Fig. 13 show an example of a two-tone suppression tuning curve for a high-CF model fiber and an actual suppression tuning curve with the same CF (Delgutte, 1990). The general shape of the AN-model suppression tuning curve is similar to those reported for AN fibers: suppression thresholds are lowest for frequencies just above CF, and there is a broad low-frequency region of suppression. These two properties were introduced into the model by shifting the center frequency of the control-path filter to a frequency slightly higher than the CF of the signal-path filter (see above). In addition to the asymmetry in thresholds above and below CF, there is an asymmetrical growth of two-tone suppression for suppressors above and below CF. This property is illustrated in the lower two panels of Fig. 13, which show the level of a tone at CF that is required to maintain a constant discharge rate (i.e., to offset the suppression) as a function of suppressor level. The suppression growth curves for suppressor frequencies above CF are shallower than for tones below CF in both model and actual AN responses (Delgutte, 1990). The asymmetry in the model responses is qualitatively correct; however, it is not as strong as in the actual responses, especially for high CFs for which the asymmetry in growth is stronger than for low-CF fibers (Delgutte, 1990). More realistic filter shapes, as opposed to the symmetrical gammatone filter, would be expected to enhance this asymmetry. Also, the model suppression at very low frequencies does not grow as high as in the actual data; this limitation may be related to the lack of a tail mechanism at low frequencies in the model.

Another illustration of the differences between two-tone suppression properties for suppressors below and above CF is provided in Fig. 14. These plots show rate-level functions for a CF-tone alone, and for a two-tone stimulus with $F1 = \mathrm{CF}$, and $F2$ either above CF [Figs. 14(a), (c)] or below CF [Figs. 14(b), (c)]. Model responses are shown for two fibers with CFs chosen to match examples from Sachs and Abbas (1976). The difference in level between the suppressor tone and the CF tone are fixed. The range of SPLs shown, and the difference in levels between tones, were chosen to yield rate-level functions comparable to the examples (note that the model fibers have lower thresholds).

The functions in Fig. 14 show several of the trends as seen in the data (Sachs and Abbas, 1976). For a suppressor above CF [Figs. 14(a), (c)], the response to the two-tone complex begins to diverge from the CF-tone response at low levels, and the growth of suppression (as both the CF tone and the suppressor are increased in level) is gradual. For a suppressor below CF [Figs. 14(b), (d)], the threshold of suppression is high with respect to that for the CF tone alone. The growth of suppression as level increases above suppression threshold is steeper for the below-CF suppressor than for the above-CF suppressor, although suppression by below-CF frequencies, especially at high levels, is not as strong in the model as in the data (as seen above, Fig. 13). The lack of low-frequency tail mechanisms may impose a limitation on the behavior of below-CF suppressors in this model. The differences between the properties of the above-

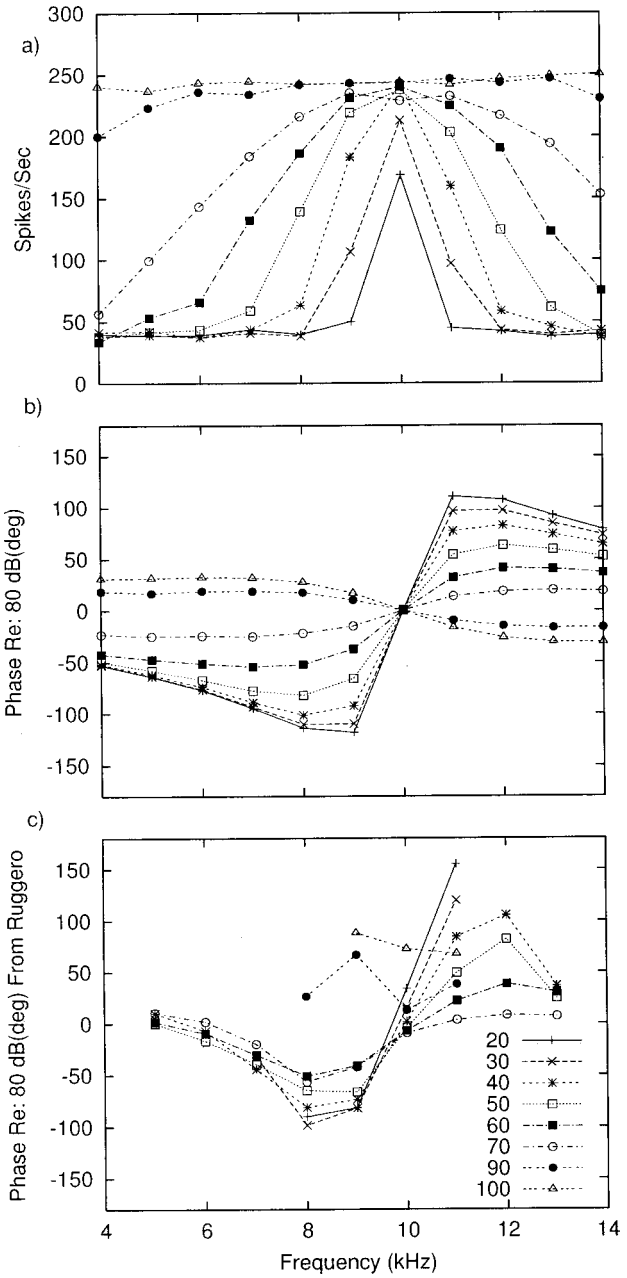

FIG. 10. Response area rates (a) and phases (b) for a model fiber with CF equal to 10 kHz. The phases are measured from the output of the signal-path filter; rolloff of phase-locking precludes using phase-locked discharge times to illustrated the level-dependent phase properties of the high-CF model fiber. Phases are referenced to the phase of the response at each frequency at 80 dB SPL, as in Ruggero *et al.* (1997). (c) For comparison, phases responses from the 10 kHz place of the basilar membrane of chinchilla (see Fig. 14 in Ruggero *et al.*, 1997; data are replotted here using the same convention as Fig. 9).

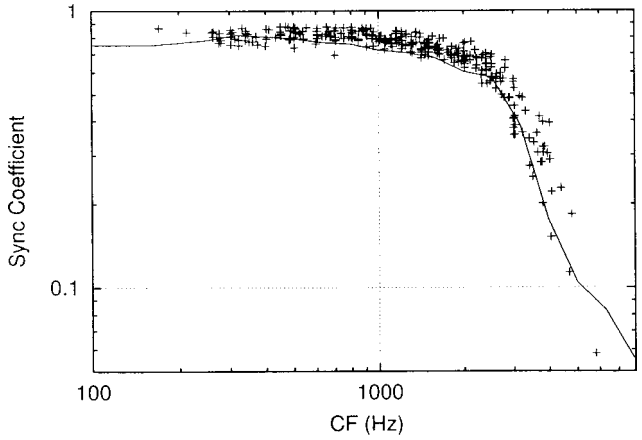

FIG. 11. Maximum synchronization coefficient of model AN fibers to CF tones as a function of CF (solid curve). Each coefficient was computed as the peak of the sync-level function (see Fig. 7) for a model fiber at each CF. The stimulus was 100 ms in duration with 3.9 ms rise/fall times. The synchronization coefficients were computed from the 10–100 ms time window referenced to the stimulus onset. Maximum synchronization coefficients for a population of AN fibers in cat (Johnson, 1980) are plotted (crosses) for comparison.

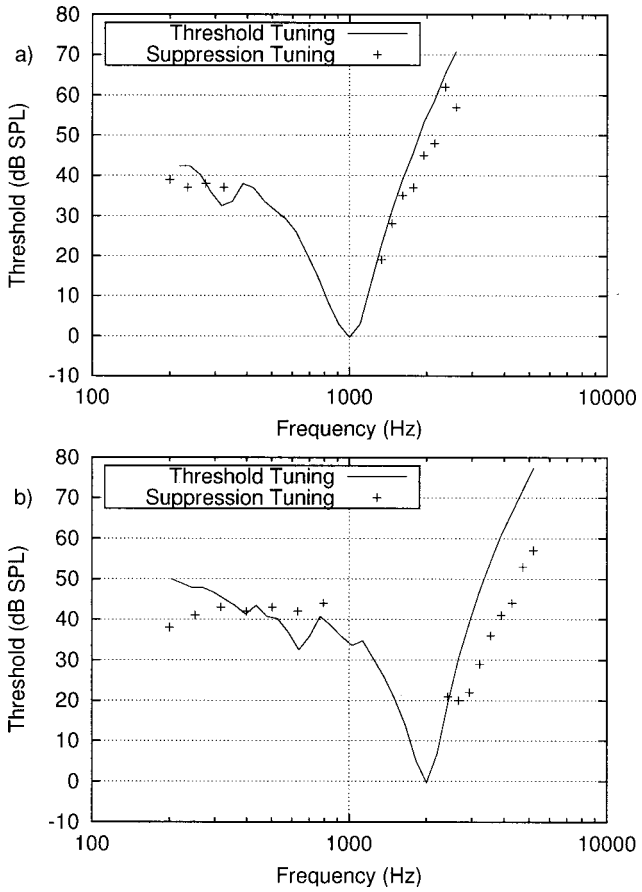

FIG. 12. Excitatory-tuning (line) and suppression-tuning (plusses) curves for model fibers with a CF at (a) 1 kHz and (b) 2 kHz. Suppression thresholds were measured using the algorithm of Delgutte (1990). Two 50 ms stimuli (combination of suppressor tone and CF tone and CF tone alone) were presented in alternation and the average discharge rate was calculated over 200 repetitions. The level of CF tone was set to produce 2/3 of the saturated rate response in the model AN fiber (typically at 20 to 25 dB SPL). The suppressor threshold was then found as the level of the suppressor that resulted in a 10 sp/s decrease in the response to the combined tones as compared to the response to the CF tone alone. The bandwidth of the suppression-tuning curve is mainly determined by the wide-band filter in the control path.

and below-CF suppressors are further illustrated by the fractional response curves (dotted lines, Fig. 14) which show the ratio between the response to the CF tone alone and the two-tone complex (Sachs and Abbas, 1976).

Addition of a suppressor tone affects not only the rate of the response to a tone at CF, but also its phase (e.g., Deng and Geisler, 1985). Figure 15(a) illustrates rate-level functions in response to $F1$ (a tone at CF, 2900 Hz) and to the two-tone complex, $F1+F2$, where $F2$ is a suppressor tone at 4700 Hz with a fixed level of 50 dB SPL. Figure 15(b)

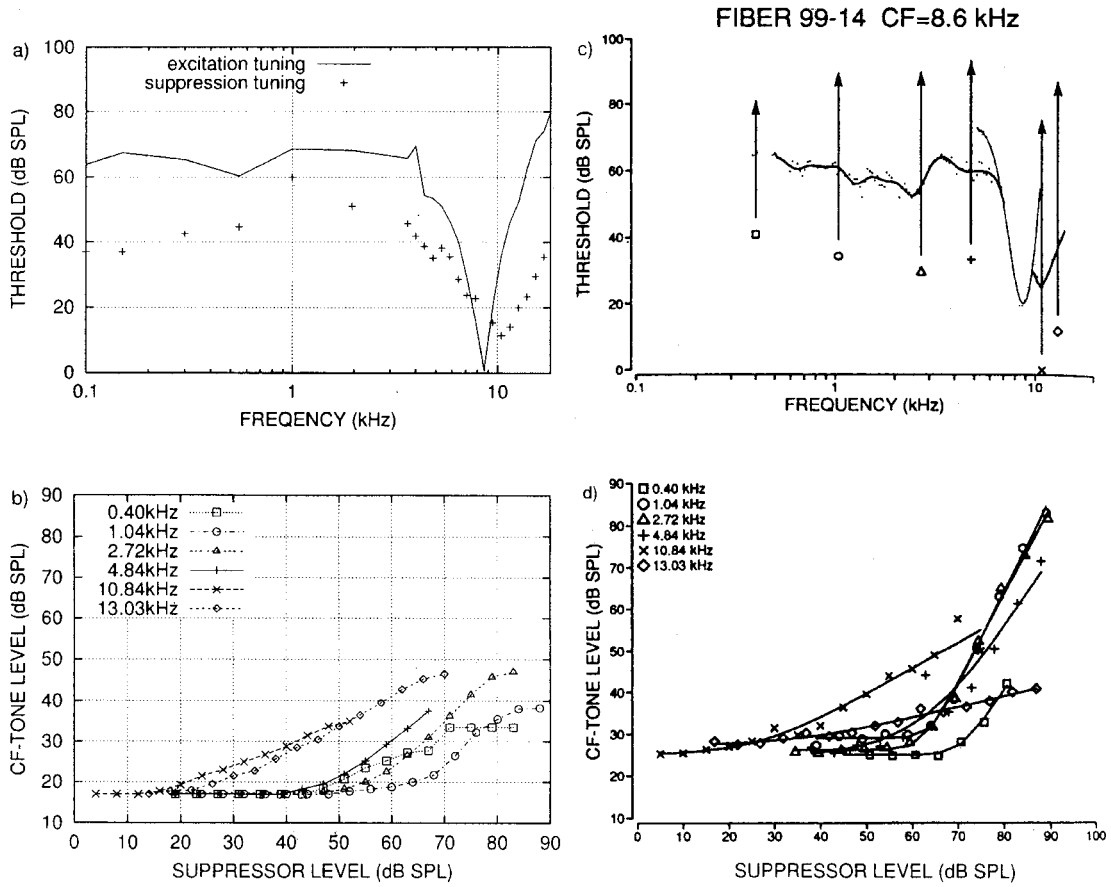

FIG. 13. Two-tone suppression tuning curve for a model fiber with CF equal to 8.6 kHz (left) in comparison to and AN fiber with the same CF (right, Delgutte, 1990; with permission). The upper panels show excitatory and suppression tuning curves (see Fig. 12 caption). The lower panels show growth of suppression for suppressors at several frequencies. The level of the CF tone required to maintain a criterion rate (2/3 of saturated rate), in the presence of the suppressor tone, is plotted as a function of the suppressor level (Delgutte, 1990). The asymmetry in high-side and low-side growth rate is comparable with experimental results from Delgutte (1990) for low-CF AN fibers, but underestimates the asymmetry for high-CF AN fibers.

shows the phase of the phase-locked responses to $F1$ alone, and the phase of the response to the $F1$ component in the two-tone complex, $F1+F2$. The trends seen in the model phase are similar to those reported by Deng and Geisler [1985, Figs. 15(c), (d)] for the majority of AN fibers. The main effect that they reported, also seen in the model response, is that addition of the suppressor $F2$ causes an increase in phase lag (where phase lag is the phase delay of the response with respect to the stimulus phase). The change in phase is seen in the response to $F1$ at levels of $F1$ where rate-suppression is seen; at higher levels of $F1$, where the model rate-level functions in response to $F1$ and $F1+F2$ converge [Figs. 15(a), (c)] the model phase functions in response to $F1$ and $F1+F2$ also converge [Figs. 15(b), (d)]; similar trends were reported for AN fibers (Deng and Geisler, 1985). Note that the change in phase with level of the model response to $F1$ is much less than for the AN data; this discrepancy is consistent with the fact that CF is level-dependent in AN fibers in this CF range while the model CF is level-independent. A change in phase in response to the CF tone of the AN fiber is also consistent with the possibility that the CF of the actual AN fiber was not exactly equal to the frequency chosen for $F1$ (whereas in the model, the CF is known); a mismatch between CF and $F1$ would result in level-dependent phase (as illustrated in Fig. 9).

The final aspect of the nonlinear response of the model to two-tone complexes illustrated here are the combination tones, or distortion products (Fig. 16). In this figure, the magnitudes of the components in the signal-path filter in response to $F1$, $F2$, and the distortion products $2F1-F2$ and $2F2-F1$, are shown. Although this filter-bank model does not provide a medium for propagation of the distortion products to the place tuned to the distortion product frequency, it is still possible to examine the trends of the low-level distortion products created by a nonlinear filter model (e.g., Goldstein, 1995). Figure 16(a) shows the response of the model's signal-path filter (shown as the magnitude of the Fourier component at the frequency of interest) to a CF tone alone, to $2F2-F1$ with $F2/F1=1.1$ and 1.2, and to $2F1-F2$, with $F2/F1=1.1$. In each case, $F1$ and $F2$ have equal amplitudes, and their frequencies are chosen such that the frequency of the combination tone is equal to the model CF of 8.5 kHz, chosen to match the CF of the example in Robles *et al.* [1991, Fig. 16(b)]. The trends in the level-dependence of both of these distortion products as a function of level, and for different $F2/F1$ ratios, are consistent with measurements from the basilar membrane. The amplitudes of the distortion products in the model are lower than those reported by Robles *et al.* (1991), which might be expected due to the fact that propagation of the distortion products and

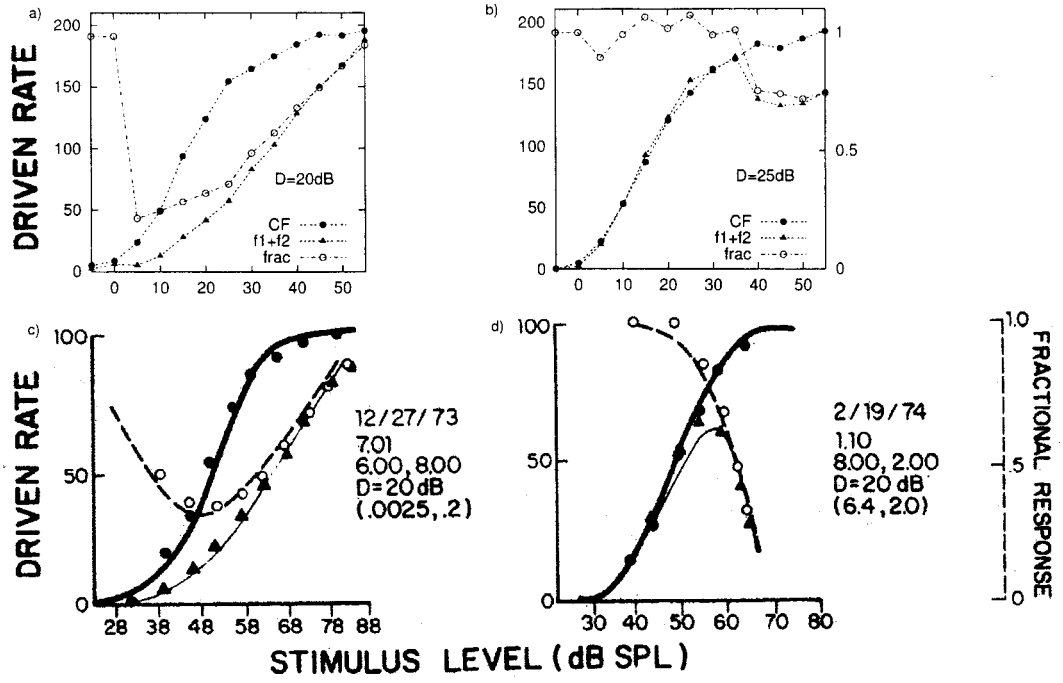

FIG. 14. Different properties of suppression for above- and below-CF suppressors. Responses of two model fibers and two AN fibers to tones at CF and two-tone complexes. (a) Model fiber with CF=6 kHz. Suppressor frequency is 8 kHz, and suppressor level is 25 dB SPL above that of the CF tone. (b) Model fiber with CF=8 kHz. Suppressor frequency is 2 kHz, and suppressor level is 20 dB SPL above that of the CF tone. (c) AN fiber from Sachs and Abbas (1976, their Fig. 4) with the same CF and suppressor parameters as the model fiber in panel a. (d) AN fiber from Sachs and Abbas (1976; with permission) with the same CF and suppressor parameters as the model fiber in panel b. Driven rate is the sustained rate (computed over the 25–45 ms window of the 60 ms duration stimulus; 500 repetitions were used) minus spontaneous rate. The fractional response (open circles) is the ratio of the driven rates in response to the CF tone and to the two-tone complex.

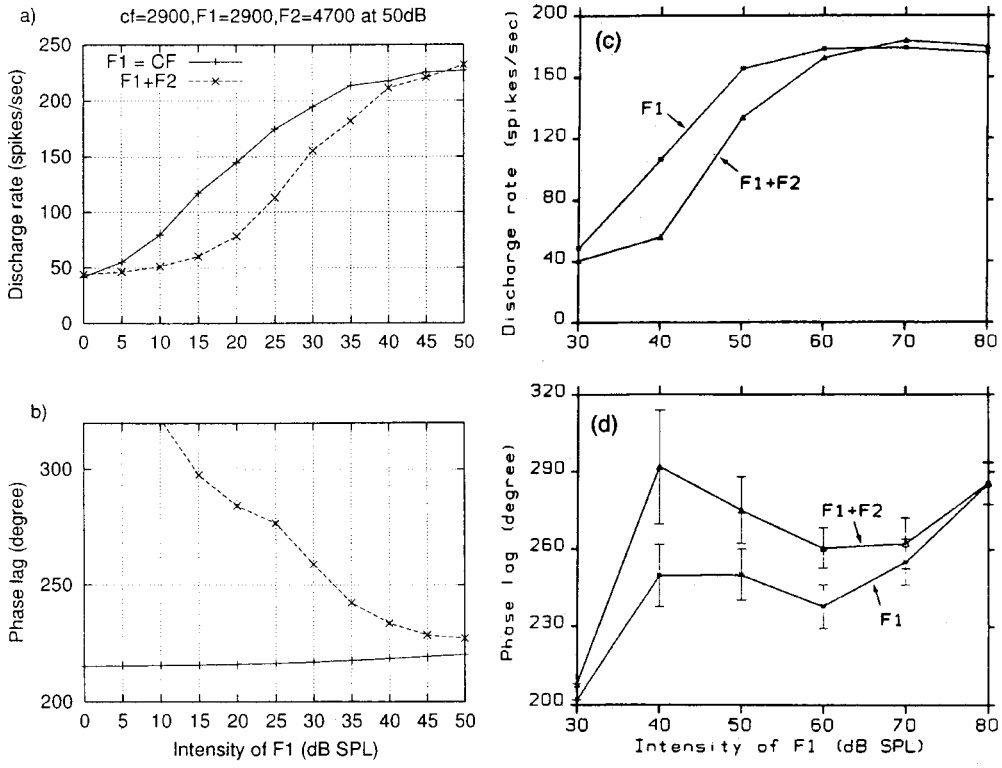

FIG. 15. Effect of a suppressor on the rate and phase of the response to a tone at CF. (a) Rate-level functions for response of model fiber with CF equal to 2900 Hz. $F1$ is at the CF, and $F2$ is 4700 Hz. The level of the tone at $F2$ is 50 dB SPL. (b) The phase of the phase-locked response to $F1$ is shown as a function of the level of the $F1$ tone. Responses are shown for responses to $F1$ alone, and for the phase of the $F1$ component of the response to $F1+F2$. (c) Rate, and (d) phase for a comparable example from Deng and Geisler (1985; with permission). The level of the suppressor in their figure was 90 dB.

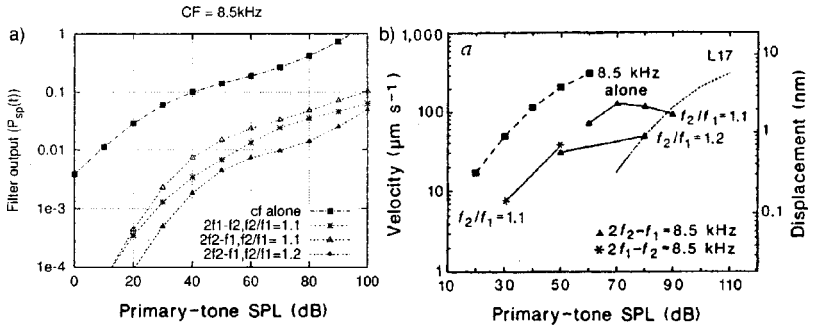

FIG. 16. (a) Amplitude of the distortion products (or combination tones) in the model response as a function of level for equal-intensity two-tone complexes. The frequencies of the primary tones were chosen so that the frequency of the distortion product (i.e., $2f1-f2$, or $2f2-f1$) was matched to the model CF (8.5 kHz). The level-dependent trends of the distortion products are similar to those measured on the basilar membrane (b) (Robles *et al.*, 1991; with permission). The amplitudes of the model distortion products are not as large as in the data, especially for the $2f1-f2$ distortion product. The low-amplitude model responses are consistent with the lack of a propagation medium in this filterbank model; the gain that would be experienced by a component as it travelled to the best place along the basilar membrane is not included here (see Goldstein, 1995).

associated amplification are not included in the model (cf. Goldstein, 1995).

Arbitrary input waveforms can be used as inputs to the model, which allows the study of the detailed temporal and statistical response properties for complex sounds. Figure 17 illustrates the temporal responses of a model fiber with a CF of 1 kHz to two broadband stimuli, clicks and wide-band noises. Both responses show periodicities in the PST histograms that are dominated by the CF of the model fiber. The representation in the model response of the envelope of the complex sound is influenced by the peripheral filtering. Representation of envelope properties in the model responses are qualitatively appropriate. A quantitative analysis of the envelope response properties of the model is not addressed here.

The empirical statistics of AN-fiber discharge counts (e.g., mean and variance) are important for evaluating potential coding schemes in the auditory nerve. Several reports (e.g., Young and Barta, 1986; Winter and Palmer, 1991) show that the empirical discharge-count statistics differ from the behavior of a Poisson process. Differences from Poisson statistics are partly due to the effects of refractoriness (Teich and Lachs, 1979). Figure 18(a) shows the mean and standard deviation of sustained-rate responses of a 1 kHz CF model

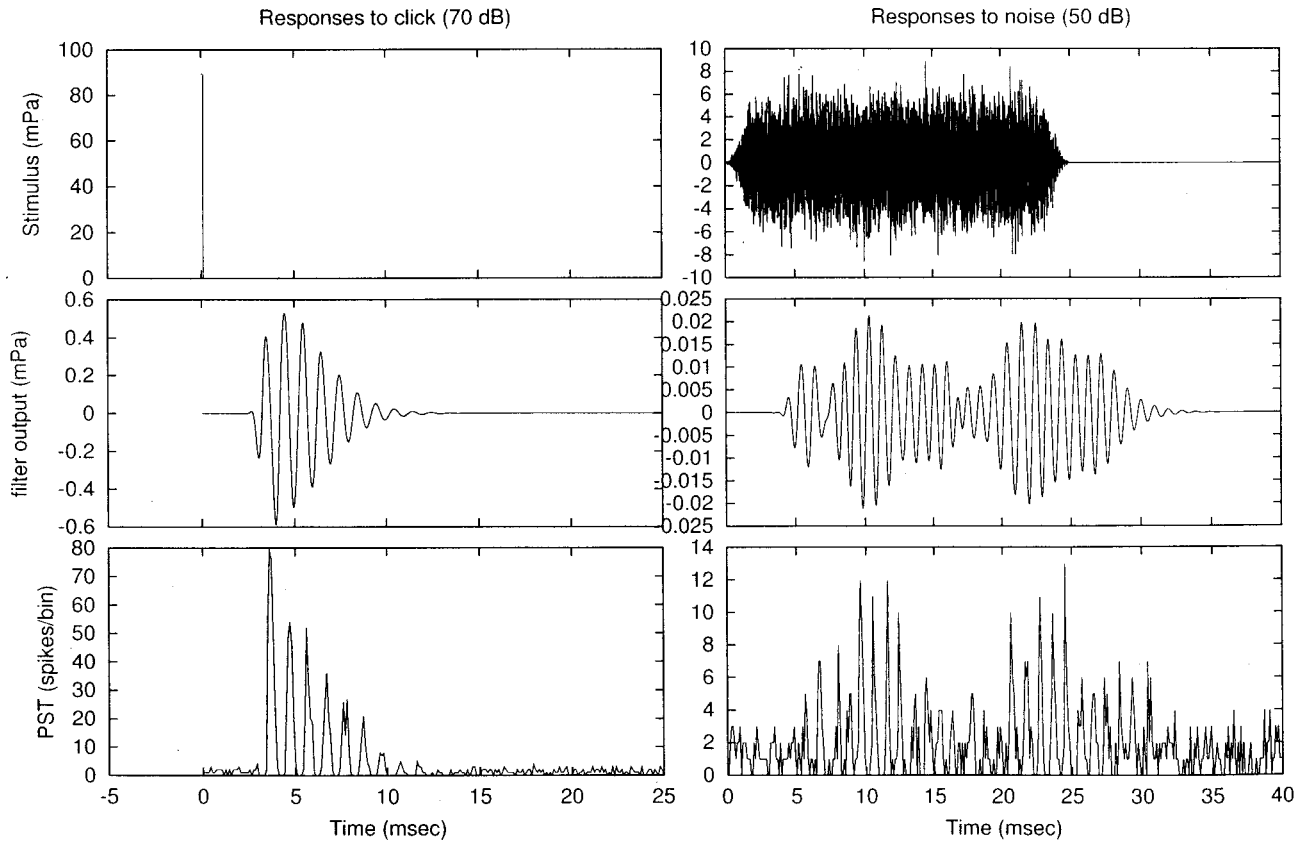

FIG. 17. Model fiber responses for CF of 1 kHz to click and noise waveforms. The top panels show the stimulus waveforms, middle panels show the response of the signal-path filter, and lower panels show PST histograms of response to 500 repetitions. The click stimulus is 200 μs long and 70 dB SPL (peak equivalent). The Gaussian noise stimulus has a bandwidth of 10 kHz and was presented at 50 dB SPL rms.

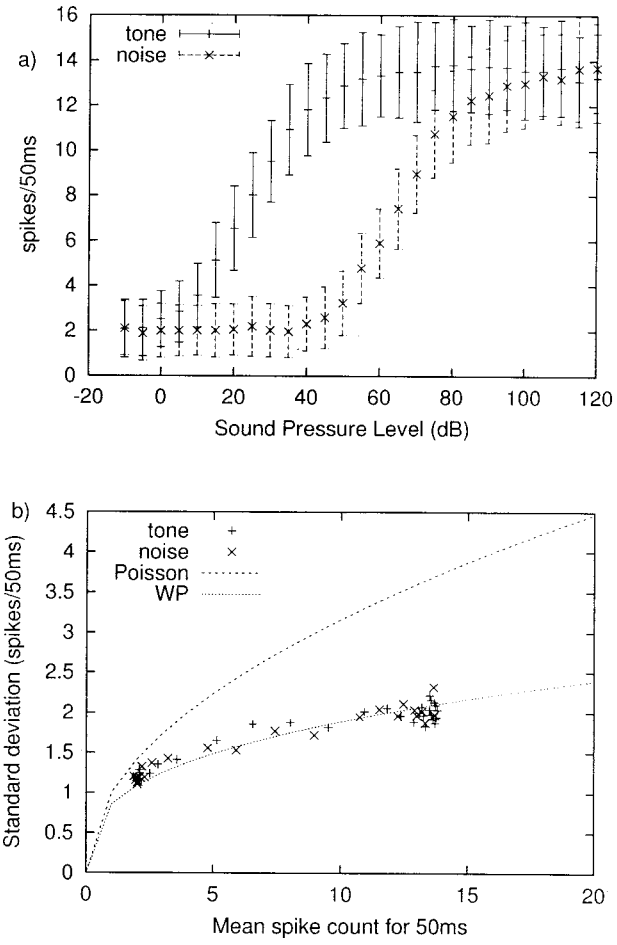

FIG. 18. (a) Rate-level functions (mean and standard deviation) for responses to tones at CF and to wide-band noises for a model fiber with a CF of 1 kHz. Discharges in the 1.25–51.25 ms time window were counted for 200 repetitions of each stimulus. The Gaussian noise stimulus has a bandwidth of 10 kHz. The responses to the noise are shifted to the right (with respect to the tone responses) because they are plotted as a function of dB SPL rms. (b) Standard deviation versus mean discharge counts for tone and noise responses. The dotted line is the fit to Young and Barta's (1986) data used by Winter and Palmer (1991), and the dashed line is the standard deviation for a Poisson process.

fiber to a CF tone and to a wide-band noise as a function of level. The model shows a wider dynamic range for noises than for tones (Schalk and Sachs, 1980; May and Sachs, 1992). Figure 18(b) shows the standard deviation of the model-response rate as a function of the mean discharge count for both CF tones (crosses) and noise (plusses). The dotted line is a fit (from Winter and Palmer, 1991) to the experimental data of Young and Barta (1986), and the dashed line is the standard deviation expected for a Poisson process. The statistical responses of the model fiber are consistent with physiological responses as summarized by the dotted line.

The revcor function is a useful estimate of the AN fiber's impulse response based on responses to wide-band noise (de Boer and de Jongh, 1978). The revcor filters estimated from model noise responses at different levels are illustrated in Fig. 19(a) and show changes in bandwidth as a function of the input level that are comparable to actual AN revcor filters [Fig. 19(b)] (Carney and Yin, 1988). The changes in bandwidth of the revcor filters are relatively small for low-CF AN fibers (cf. Evans, 1977; de Boer and de Jongh, 1978; Carney and Yin, 1988) due to the relatively small gain of the cochlear amplifier at low CFs. However, the level-dependent changes in phase near the CF (Fig. 19) associated with these changes in bandwidth represent significant level-dependent temporal shifts of the AN discharge times at low frequencies that have been hypothesized to be important for level encoding (Carney, 1994). Recent studies have quantified the information contained in these nonlinear temporal response properties and have shown that they contribute significant information for level encoding that is not included in the average-rate responses of the majority of AN fibers (Heinz *et al.*, 1999, 2001; Colburn *et al.*, 2001).

IV. DISCUSSION

This report describes a phenomenological model for AN responses that includes the major nonlinearities associated with the cochlear amplifier. The model has compressive gain in response to tones at CF, nonlinear bandwidth and phase, and two-tone suppression. The model has asymmetric growth of two-tone suppression, i.e., suppression-growth is greater for tones below CF than for tones above CF. This property has been difficult to incorporate into previous models that predict responses to arbitrary stimuli (Delgutte, 1990). Other aspects of the model discharge properties for high-spontaneous-rate fibers are also appropriate, including saturating rate-level functions, the drop in synchrony as a function of CF, and the statistical nature of discharge counts across a range of discharge rates. The responses of this model to a wide range of simple and complex stimuli provide reasonably accurate representations of the discharge rates and discharge times of AN fibers across a wide range of CFs and levels.

Physiological data show that the active process of the basilar membrane is affected by a wide region of the basilar membrane (Delgutte, 1990; Zhao and Santos-Sacchi, 1999). It has also been shown that tones at frequencies above and below CF have different effects on nonlinear tuning (Delgutte, 1990; Ruggero *et al.*, 1992). Experimental data on IHCs and AN suppression tuning curves also suggest that the OHCs responsible for enhancing vibration of a group of IHCs are located basal to the IHCs (Patuzzi, 1996). The current model's time-varying wide-band filter in the control path, which is shifted slightly basal to the AN-fiber CF, is used to represent the effect of the local and neighboring OHCs on responses of the signal-path filter.

Several AN response properties were not included in this model and are challenges for future modeling studies. For example, the model does not include tails of tuning curves (Kiang and Moxon, 1974; Liberman and Kiang, 1978), the glide in instantaneous frequency in the AN impulse response that is related to the level-dependent shift in best frequency (Carney *et al.*, 1999), the dramatic changes in rate and phase in response to tones (i.e., simple-tone interference) and clicks at high sound levels (Kiang, 1990; Ruggero *et al.*, 1996; Lin and Guinan, 2000), the effects of middle- and external-ear acoustics (Rosowski, 1996), the effects of efferents on the rate and timing of AN discharges (Wiederhold, 1986; Guinan, 1996), and low and medium

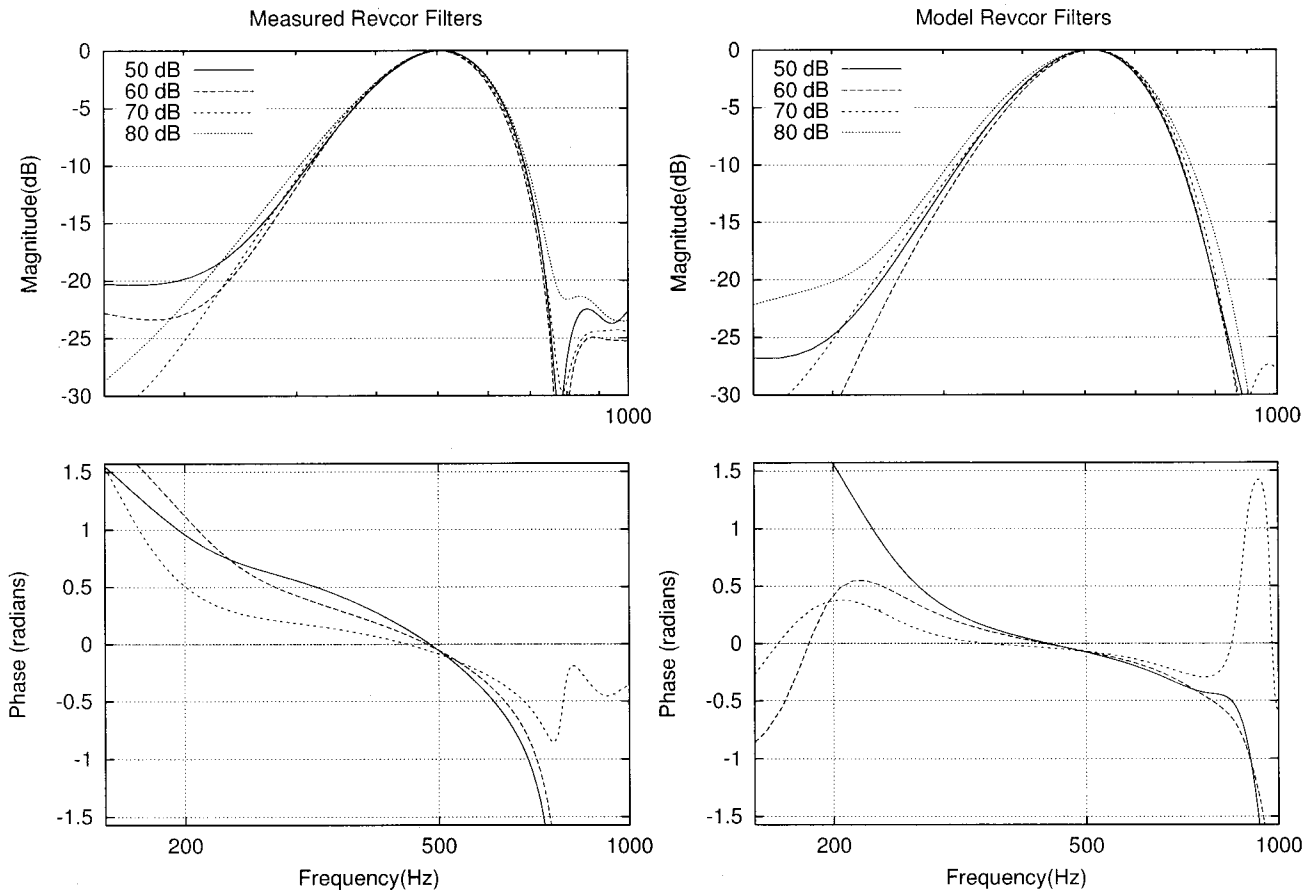

FIG. 19. (a) Spectral magnitude and phase of the revcor filters of a model fiber with CF of 510 Hz measured from responses to wide-band noise presented at several levels. The functions were calculated by averaging 15 ms of the stimulus prior to each discharge time that resulted from a 10 s noise stimulus presented for five repetitions. A Hamming window was used to calculate the frequency responses. The amplitudes of the filter responses were normalized to 0 dB at CF (Carney, 1993; Carney and Yin, 1988). Noise levels are given in dB SPL rms. (b) Examples of revcor functions at several levels for actual cat AN fiber with CF equal to 510 Hz (Unit ID: U86166-39, recorded as part of a previous study; Carney and Yin, 1988).

spontaneous rates (Liberman, 1978). In addition, as discussed above, the filterbank nature of this phenomenological model precludes explanation of phenomena that depend upon propagation of signals along the basilar membrane, such as the overall phase properties and propagation of combination tones to the position along the basilar membrane tuned to the distortion tones (see Goldstein, 1990, for a description of this limitation).

Inclusion of the tails of the tuning curves may play an important role in understanding population responses to moderate- to high-level broadband stimuli, such as speech sounds, in which significant energy at low frequencies may influence responses of neurons over a wide range of CFs. Also, the glide in the instantaneous frequency of the impulse responses will influence both the rate and timing of discharges for most AN fibers over a wide range of stimulus levels. Because this property interacts with the nonlinear tuning to produce shifts in frequency tuning with sound level (Recio *et al.*, 1996; Carney *et al.*, 1999), this property is important to explore in future models that include nonlinear tuning.

The model described here represents a significant extension of our previous modeling efforts (Carney, 1993) in that the nonlinear tuning is much more accurate without a significant increase in the complexity of the model, and the model has been extended to high CFs. The gain and bandwidth of each AN fiber were influenced by a broad frequency range surrounding the fiber's CF, which resulted in more accurate two-tone suppression. One aspect of the two-tone suppression property that was not accurately captured in this model was the degree of asymmetry in the growth of suppression with suppressor level. The asymmetry of the model is similar to that described for low-CF fibers, but not as strong as reported for high-CF fibers (Delgutte, 1990). A future model that includes CF-dependent shifts in frequency with level, in both the signal path and the control path, might be able to accurately simulate this aspect of two-tone suppression. Inclusion of the CF-dependent glide in the instantaneous frequency of the impulse responses (Carney *et al.*, 1999) may be sufficient to make this aspect of two-tone suppression more accurate. In addition, interactions between mechanisms for two-tone interaction and tail mechanisms in future models would be expected to influence the asymmetry of growth of suppression.

Extension of this model to include low- and medium-spontaneous-rate fibers is motivated by the need for accurate descriptions of these responses to examine their potential role in level encoding of pure tones, as well as complex sounds. It is also important to explore the different spontaneous-rate groups in the context of a nonlinear model,

since the slopes and dynamic ranges of their rate-level functions are strongly influenced by the cochlear amplifier (e.g., Yates *et al.*, 1992). In addition, the ability of this model to simulate responses over a wide range of CFs is important to the further study of models for AN fibers with different spontaneous rates. The change in the amount of compression (or equivalently, the change in the gain of the cochlear amplifier) as a function of CF has strong implications for the roles of the different spontaneous-rate fibers in encoding stimulus features at different CFs (Heinz *et al.*, 1999, 2001). A nonlinear model for AN responses over a wide range of CFs and spontaneous rates will allow quantification of the information encoded by these fibers (e.g., Colburn *et al.*, 2001).

Another direction for extension of this model is to combine the nonlinear filterbank approach used here with some aspects of the parallel signal-processing pathways of the MBPNL approach. Such an effort might allow explanation of a wider range of phenomena than can be explained by either model independently. The tails of tuning curves (Goldstein, 1990), the multiple modes of excitation that are suggested by Lin and Guinan's (2000), and the level-dependent phase relationship between tip and tail phenomena suggested by these and other AN responses (e.g., Goblick and Pfeiffer, 1969; Lin and Goldstein, 1995) are examples of phenomena that could be approached by combining aspects of these two modeling approaches. The present modeling approach provides a useful description of both rate and temporal (including nonlinear phase) response properties from excitation modes associated with the active cochlear process, while the MBPNL approach provides a valuable framework for modeling response properties associated with the combination of multiple modes (either active or passive).

ACKNOWLEDGMENTS

We acknowledge the helpful comments of Susan Moscynski on earlier versions of this manuscript, and of Susan Early on later versions. Dr. Roger Miller generously provided the Q10 data in Fig. 3. Dr. Don Johnson generously provided the synchronization coefficients illustrated in Fig. 12. Dr. Mario Ruggero generously provided the basilar membrane phase data plotted in Fig. 11. Dr. Philip Joris provided unpublished plots of synchronization coefficient versus SPL for a number of mid-frequency AN fibers, which were critical for modification of the IHC model. Dr. Ray Meddis provided helpful comments in a review of the manuscript, and Dr. Julius Goldstein generously provided detailed information on the MBPNL model. This work was supported by the Office of Naval Research Grant Agmt No. Z883402 (XZ, MGH, LHC), NIH T32DC00038 (MGH), NIDCD DC00109 (ICB), and NIDCD DC00023(ICB).

APPENDIX

The IHC-AN synapse model is a time-varying implementation of Westerman and Smith's (1988) three-store diffusion model that allows simulations of responses to arbitrary stimuli. The three stores are the immediate (I), local (L), and global (G) stores. The concentration (C) at each store varies as the ''substance'' to be released diffuses; the concentration differences and the permeability (P) at each boundary regulate the rate of diffusion.

The local and global permeabilities and the three volumes are constant values; these values are specified in terms of time constants for diffusion and response amplitudes that can be estimated from the literature and adjusted based on the shape of the model's PST histogram. The desired response properties, based on PST histograms in response to tones, are used to set the parameter values for the steady-state discharge rate, A_{SS}; spontaneous rate, *spont*; rapid time constant for adaptation, τ_R; short-term time constant for adaptation, τ_{ST}; the ratio of rapid response amplitude to short-term response amplitude, $A_{R/ST}$; the maximum immediate permeability, $P_{I\,\max}$; and the peak-to-sustained response amplitude ratio, PTS.

Several intermediate parameters can then be determined from those above. The onset rate, rapid and short-term response amplitudes, resting permeability and global concentration are computed as follows:

$$A_{\mathrm{ON}}=\mathrm{PTS}\,A_{SS}, \tag{A1}$$

$$A_R=(A_{\mathrm{ON}}-A_{SS})\frac{A_{R/ST}}{(1+A_{R/ST})}, \tag{A2}$$

$$A_{ST}=A_{\mathrm{ON}}-A_{SS}-A_R, \tag{A3}$$

$$P_{\mathrm{rest}}=P_{I\,\max}\frac{spont}{A_{\mathrm{ON}}}, \tag{A4}$$

$$C_G=\frac{spont(A_{\mathrm{ON}}-spont)}{A_{\mathrm{ON}}P_{\mathrm{rest}}(1-spont/A_{SS})}. \tag{A5}$$

The volumes of the three stores are then computed; first several intermediate parameters are defined as (see Westerman and Smith, 1988):

$$\gamma_1=C_G/spont,\quad \gamma_2=C_G/A_{SS},$$
$$\kappa_1=-1/\tau_R,\quad \kappa_2=-1/\tau_{ST}. \tag{A6}$$

Following the strategy of Westerman and Smith (1988), the immediate volume is computed as:

$$V_{I0}=\frac{1-P_{I\,\max}/P_{\mathrm{rest}}}{\gamma_1\{[A_R(\kappa_1-\kappa_2)/(C_GP_{I\,\max})]+\kappa_2/(P_{\mathrm{rest}}\gamma_1)-\kappa_2/(P_{I\,\max}\gamma_2)\}}, \tag{A7}$$

$$V_{I1}=\frac{1-P_{I\,\max}/P_{\mathrm{rest}}}{\gamma_1\{[A_{ST}(\kappa_2-\kappa_1)/(C_GP_{I\,\max})]+\kappa_1/(P_{\mathrm{rest}}\gamma_1)-\kappa_1/(P_{I\,\max}\gamma_2)\}}, \tag{A8}$$

$$V_I=\frac{V_{I0}+V_{I1}}{2}. \tag{A9}$$

Several other intermediate parameters are useful for the derivation of the other volumes and permeabilities:

$$\alpha = \frac{\gamma_2}{\kappa_1 \kappa_2}, \quad \beta = -(\kappa_1 + \kappa_2)\alpha, \quad \theta_1 = \alpha P_{I\,\max}/V_I,$$
$$\theta_2 = V_I/P_{I\,\max}, \quad \theta_3 = \gamma_2 - 1/P_{I\,\max}. \tag{A10}$$

Then, the local and global permeabilities can be specified as:

$$P_L = \left(\frac{\beta - \theta_2\theta_3}{\theta_1} - 1\right) P_{I\,\max}, \tag{A11}$$

$$P_G = \frac{1}{\theta_3 - 1/P_L}. \tag{A12}$$

The local volume and concentration, and the resting value of the immediate concentration, are set as follows:

$$V_L = \theta_1 P_L P_G, \tag{A13}$$

$$C_{I\,\mathrm{rest}} = spont/P_{\mathrm{rest}}, \tag{A14}$$

$$C_{L\,\mathrm{rest}} = C_{I\,\mathrm{rest}} \frac{(P_{\mathrm{rest}} + P_L)}{P_L}. \tag{A15}$$

The voltage-dependent immediate permeability, P_I varies with the IHC-model voltage, V_{IHC}, through a soft-rectifier specified as:

$$P_I(t) = \frac{P_{SL}}{P_{ST}} \log(1 + e^{P_{ST} V_{\mathrm{IHC}}(t)})$$
$$\text{where} \quad P_{SL} = P_{\mathrm{rest}} P_{ST}/\log(2)$$
$$\text{and} \quad P_{ST} = \log(2^{V_{\mathrm{sat}}/P_{\mathrm{rest}}} - 1), \tag{A16}$$

where P_{rest} is the resting value of the immediate permeability, and V_{sat} sets the saturation voltage for the soft rectifier. The value of V_{sat} varies with CF, in order to maintain the threshold of the model fibers at about 0 dB SPL at CF:

$$V_{\mathrm{sat}}(\mathrm{CF}) = 18.54\, P_{I\,\max} K_{\mathrm{CF}}$$
$$\text{where} \quad K_{\mathrm{CF}} = \max[1.5, 2 + 3\log_{10}(\mathrm{CF}/1000)]. \tag{A17}$$

Note that Eqs. (17) and (18) in the text provide simple numerical descriptions for the IHC-synapse model expressions shown above; p_1 in the text is equivalent to P_{SL}/P_{ST} and p_2 is equal to P_{ST}.

The difference equations for the concentrations of the stores in the diffusion model are as follows:

$$C_I(kT+T) = C_I(kT) + \frac{T}{V_I}\{[-P_I(kT)C_I(kT)] + P_L[C_L(kT) - C_I(kT)]\}, \tag{A18}$$

$$C_L(kT+T) = C_L(kT) + \frac{T}{V_L}\{-P_L[C_L(kT) - C_I(kT)] + P_G[C_G - C_L(kT)]\}, \tag{A19}$$

where T is the sampling time used in the simulation. The initial values are set as follows: $C_I(0) = C_{I\,\mathrm{rest}}$, $C_L(0) = C_{L\,\mathrm{rest}}$, and $P_I(0) = P_{\mathrm{rest}}$. Finally, the output of the synapse model is:

$$S(kT) = C_I(kT)\, P_I(kT). \tag{A20}$$

[1]The code will be made available on the Earlab website at Boston University: http://earlab.bu.edu

[2]The order of this low-pass filter influences the strength of harmonic distortions in the model responses. For filter orders less than three, the harmonic distortions seen in the tuning curves and response areas are much stronger than those observed in reports of these measures in the literature of AN responses (e.g., Kiang *et al.*, 1965; Anderson *et al.*, 1971; Rose *et al.*, 1971; Liberman, 1978).

Anderson, D. J., Rose, J. E., Hind, J. E., and Brugge, J. F. (**1971**). ''Temporal position of discharges in single auditory nerve fibers within the cycle of a sine-wave stimulus: Frequency and intensity effects,'' J. Acoust. Soc. Am. **49**, 1131–1139.

Arthur, R. M., Pfeiffer, R. R., and Suga, N. (**1971**). ''Properties of two-tone inhibition in primary auditory neurones,'' J. Physiol. **212**, 593–609.

Carney, L. H. (**1990**). ''Sensitivities of cells in the anteroventral cochlear nucleus of cat to spatio-temporal discharge patterns across primary afferents,'' J. Neurophysiol. **64**, 437–456.

Carney, L. H. (**1993**). ''A model for the responses of low-frequency auditory-nerve fibers in cat,'' J. Acoust. Soc. Am. **93**, 401–417.

Carney, L. H. (**1994**). ''Spatiotemporal encoding of sound level: Models for normal encoding and recruitment of loudness,'' Hear. Res. **76**, 31–44.

Carney, L. H., and Yin, T. C. T. (**1988**). ''Temporal coding of resonances by low-frequency auditory nerve fibers: Single-fiber responses and a population model,'' J. Neurophysiol. **60**, 1653–1677.

Carney, L. H., McDuffy, M. J., and Shekhter, I. (**1999**). ''Frequency glides in the impulse responses of auditory-nerve fibers,'' J. Acoust. Soc. Am. **105**, 2384–2391.

Cheatham, M. A., and Dallos, P. (**1989**). ''Two-tone suppression in inner hair cell responses,'' Hear. Res. **40**, 187–196.

Cheatham, M. A., and Dallos, P. (**1990**). ''Comparisons of low- and high-side two-tone suppression in inner hair cell and organ of corti responses,'' Hear. Res. **50**, 193–210.

Cheatham, M. A., and Dallos, P. (**1992**). ''Two-tone suppression in inner hair cell responses: Correlates of rate suppression in the auditory nerve,'' Hear. Res. **60**, 1–12.

Cheatham, M. A., and Dallos, P. (**1993**). ''Longitudinal comparisons of IHC ac and dc receptor potentials recorded from the guinea pig cochlea,'' Hear. Res. **68**, 107–114.

Cheatham, M. A., and Dallos, P. (**1998**). ''The level dependence of response phase: Observations from cochlear hair cells,'' J. Acoust. Soc. Am. **104**, 356–369.

Cheatham, M. A., and Dallos, P. (**1999**). ''Response phase: A view from the inner hair cell,'' J. Acoust. Soc. Am. **105**, 799–810.

Colburn, H. S., Carney, L. H., and Heinz, M. G. (**2001**). ''Quantifying the information in auditory-nerve responses for level discrimination,'' J. Assoc. Res. Otolaryngol. (submitted).

Cooper, N. P. (**1996**). ''Two-tone suppression in cochlear mechanics,'' J. Acoust. Soc. Am. **99**, 3087–3098.

Cooper, N. P., and Rhode, W. S. (**1996**). ''Two-tone suppression in apical cochlear mechanics,'' Aud. Neurosci. **3**, 123–134.

Cooper, N. P., and Rhode, W. S. (**1997**). ''Mechanical responses to two-tone distortion products in the apical and basal turns of the mammalian cochlea,'' J. Neurophysiol. **78**, 261–270.

Costalupes, J. A., Rich, N. C., and Ruggero, M. A. (**1987**). ''Effects of excitatory and non-excitatory suppressor tones on two-tone rate suppression in auditory nerve fibers,'' Hear. Res. **26**, 155–164.

Dallos, P. (**1985**). ''Response characteristics of mammalian cochlear hair cells,'' J. Neurosci. **5**, 1591–1608.

de Boer, E. (**1975**). ''Synthetic whole-nerve action potentials for the cat,'' J. Acoust. Soc. Am. **58**, 1030–1045.

de Boer, E., and Krudenier, C. (**1990**). ''On ringing limits of the auditory periphery,'' Biol. Cybern. **63**, 433–442.

de Boer, E., and de Jongh, H. R. (**1978**). ''On cochlear encoding: Potentialities and limitations of the reverse correlation technique,'' J. Acoust. Soc. Am. **63**, 115–135.

de Boer, E., and Nuttall, A. L. (**1997**). ''The mechanical waveform of the basilar membrane. I. Frequency modulations (''glides'') in impulse responses and cross-correlation functions,'' J. Acoust. Soc. Am. **101**, 3583–3592.

Delgutte, B. (**1990**). ''Two-tone rate suppression in auditory-nerve fibers: Dependence on suppressor frequency and level,'' Hear. Res. **49**, 225–246.

Deng, L., and Geisler, C. D. (**1985**). ''Changes in phase of excitor-tone

responses in cat auditory-nerve fibers by suppressor tones and fatigue,'' J. Acoust. Soc. Am. **78**, 1633–1643.
Deng, L., and Geisler, C. D. (**1987**). ''A composite model for processing speech sounds,'' J. Acoust. Soc. Am. **82**, 2001–2012.
Duifhuis, H. (**1976**). ''Cochlear nonlinearity and second filter: Possible mechanism and implications,'' J. Acoust. Soc. Am. **67**, 914–927.
Evans, E. F. (**1977**). ''Frequency selectivity at high signal levels of single units in cochlear nerve and nucleus,'' in *Psychophysics and Physiology of Hearing*, edited by E. F. Evans and J. P. Wilson (Academic, New York), pp. 185–192.
Geisler, C. D. (**1990**). ''Evidence for expansive power functions in the generation of the discharges of 'low- and medium-spontaneous' auditory-nerve fibers,'' Hear. Res. **44**, 1–12.
Geisler, C. D., and Rhode, W. D. (**1982**). ''The phases of basilar membrane vibrations,'' J. Acoust. Soc. Am. **71**, 1201–1203.
Geisler, C. D., and Sinex, D. G. (**1980**). ''Responses of primary auditory fibers to combined noise and tonal stimuli,'' Hear. Res. **3**, 317–334.
Giguere, C., and Woodland, P. C. (**1994**). ''A computational model of the auditory periphery for speech and hearing research. I. Ascending path,'' J. Acoust. Soc. Am. **95**, 331–342.
Goblick, Jr., T. J., and Pfeiffer, R. R. (**1969**). ''Time-domain measurements of cochlear nonlinearities using combination click stimuli,'' J. Acoust. Soc. Am. **46**, 924–938.
Goldstein, J. L. (**1990**). ''Modeling rapid waveform compression on the basilar membrane as multiple-bandpass-nonlinearity filtering,'' Hear. Res. **49**, 39–60.
Goldstein, J. L. (**1995**). ''Relations among compression, suppression, and combination tones in mechanical responses of the basilar membrane: Data and MBPNL model,'' Hear. Res. **89**, 52–68.
Guinan, Jr., J. J. (**1996**). ''Physiology of olivocochlear efferents,'' in *The Cochlea*, edited by P. Dallos, A. N. Popper, and R. R. Fay (Springer, New York), pp. 435–502.
Heinz, M. G., Colburn, H. S., and Carney, L. H. (**1999**). ''Monaural, cross-frequency coincidence detection as a mechanism for decoding perceptual cues provided by the cochlear amplifier,'' (Abstract) J. Acoust. Soc. Am. **105**, 1023.
Heinz, M. G., Colburn, H. S., and Carney, L. H. (**2001**). ''Monaural cross-frequency coincidence detection for level discrimination: Decoding rate and timing cues associated with the cochlear amplifier,'' J. Acoust. Soc. Am. (submitted).
Hewitt, M. J., and Meddis, R. (**1991**). ''An evaluation of eight computer models of mammalian inner hair-cell function,'' J. Acoust. Soc. Am. **90**, 904–917.
Hicks, M. L., and Bacon, S. P. (**1999**). ''Psychophysical measures of auditory nonlinearities as a function of frequency in individuals with normal hearing,'' J. Acoust. Soc. Am. **105**, 326–338.
Holley, M. C. (**1996**). ''Outer hair cell motility,'' in *The Cochlea*, edited by P. Dallos, A. N. Popper, and R. R. Fay (Springer-Verlag, New York), pp. 386–434.
Irino, T., and Patterson, R. D. (**1997**). ''A time-domain level-dependent auditory filter: The gammachirp,'' J. Acoust. Soc. Am. **101**, 412–419.
Javel, E., Geisler, C. D., and Ravindran, A. (**1978**). ''Two-tone suppression in auditory nerve of the cat: Rate-intensity and temporal analyses,'' J. Acoust. Soc. Am. **63**, 1093–1104.
Javel, E., McGee, J., Walsh, E. J., Farley, G. R., and Gorga, M. P. (**1983**). ''Suppression of auditory nerve responses. II. Suppression threshold and growth, iso-suppression contours,'' J. Acoust. Soc. Am. **74**, 801–813.
Jenison, R. L., Greenberg, S., Kluender, K. R., and Rhode, W. S. (**1991**). ''A composite model of the auditory periphery for the processing of speech based on the filter response functions of single auditory-nerve fibers,'' J. Acoust. Soc. Am. **90**, 773–786.
Johannesma, P. I. M. (**1972**). The pre-response stimulus ensemble of neurons in the cochlear nucleus,'' in *Proceedings of the Symposium on Hearing Theory* (IPO, Eindhoven, The Netherlands), pp. 58–69.
Johnson, D. H. (**1980**). ''The relationship between spike rate and synchrony in responses of auditory-nerve fibers to single tones,'' J. Acoust. Soc. Am. **68**, 1115–1122.
Joris, P. (**1999**) (personal communication).
Kiang, N. Y. S. (**1975**). ''Stimulus representation in the discharge patterns of auditory neurons,'' in *The Nervous System, Vol. 3: Human Communication and Its Disorders*, edited by D. B. Tower (Raven, New York), pp. 81–95.
Kiang, N. Y. S. (**1990**). ''Curious oddments of auditory-nerve studies,'' Hear. Res. **49**, 1–16.
Kiang, N. Y. S., and Moxon, E. C. (**1974**). ''Tails of tuning curves of auditory-nerve fibers,'' J. Acoust. Soc. Am. **55**, 620–630.
Kiang, N. Y. S., Watanabe, T., Thomas, E. C., and Clark, L. F. (**1965**). *Discharge Patterns of Single Fibers in the Cat's Auditory Nerve*, M.I.T. Research Monograph 35 (MIT Press, Cambridge).
Liberman, M. C. (**1978**). ''Auditory-nerve responses from cats raised in a low-noise chamber,'' J. Acoust. Soc. Am. **63**, 442–455.
Liberman, M. C. (**1982**). ''The cochlear frequency map for the cat: Labelling auditory-nerve fibers of known characteristic frequency,'' J. Acoust. Soc. Am. **72**, 1441–1449.
Liberman, M. C., and Kiang, N. Y. S. (**1978**). ''Acoustic trauma in cats: Cochlear pathology and auditory-nerve activity,'' Acta Oto-Laryngol., Suppl. **358**, 1–63.
Lin, T., and Goldstein, J. L. (**1995**). ''Quantifying 2-factor phase relations in nonlinear responses from low characteristic-frequency auditory-nerve fibers,'' Hear. Res. **90**, 126–138.
Lin, T., and Guinan, Jr., J. J. (**2000**). ''Auditory-nerve-fiber responses to high-level clicks: Interference patterns indicate that excitation is due to the combination of multiple drives,'' J. Acoust. Soc. Am. **107**, 2615–2630.
Lopez-Poveda, E. A., O'Mard, L. P., and Meddis, R. (**1998**). ''A revised computational inner hair cell model,'' in *Psychophysical and Physiological Advances in Hearing*, edited by A. R. Palmer, A. Rees, A. Q. Summerfield, and R. Meddis (Whurr, London), pp. 112–121.
May, B. J., and Sachs, M. B. (**1992**). ''Dynamic range of neural rate responses in the ventral cochlear nucleus of awake cats,'' J. Neurophysiol. **68**, 1589–1602.
Meddis, R. (**1986**). ''Simulation of mechanical to neural transduction in the auditory receptor,'' J. Acoust. Soc. Am. **79**, 702–711.
Meddis, R. (**1988**). ''Simulation of auditory-neural transduction: Further studies,'' J. Acoust. Soc. Am. **83**, 1056–1063.
Miller, R. L., Schilling, J. R., Franck, K. R., and Young, E. D. (**1997**). ''Effects of acoustic trauma on the representation of the vowel /ɛ/ in cat auditory nerve fibers,'' J. Acoust. Soc. Am. **101**, 3602–3616.
Mountain, D. C., and Hubbard, A. E. (**1996**). ''Hair cell and auditory nerve,'' in *Auditory Computation*, edited by H. L. Hawkins, T. A. McMullen, A. N. Popper, and R. R. Fay (Springer-Verlag, New York), pp. 121–156.
Narayan, S. S., Temchin, A. N., Recio, A., and Ruggero, M. A. (**1998**). ''Frequency tuning of basilar membrane and auditory nerve fibers in the same cochleae,'' Science **282**, 1882–1884.
Nomoto, M., Suga, N., and Katsuki, Y. (**1964**). ''Discharge pattern and inhibition of primary auditory nerve fibers in the monkey,'' J. Neurophysiol. **27**, 768–787.
Nuttall, A. L., and Dolan, D. F. (**1993**). ''Two-tone suppression of inner hair cell and basilar membrane responses in the guinea-pig,'' J. Acoust. Soc. Am. **93**, 390–400.
Nuttall, A. L., and Dolan, D. F. (**1996**). ''Steady-state sinusoidal velocity responses of the basilar membrane in guinea pig,'' J. Acoust. Soc. Am. **99**, 1556–1564.
Oppenheim, A. V., and Schafer, R. W. (**1975**). *Digital Signal Processing* (Prentice-Hall, Englewood Cliffs, NJ).
Palmer, A. R., and Russell, I. J. (**1986**). ''Phase-locking in the cochlear nerve of the guinea-pig and its relation to the receptor potential of inner hair cell,'' Hear. Res. **24**, 1–15.
Patterson, R. D., Nimmo-Smith, I., Holdsworth, J., and Rice, P. (**1988**). ''Implementing a gammatone filter bank,'' SVOS Final Report: The Auditory Filter Bank.
Patuzzi, R. (**1996**). ''Cochlear micromechanics and macromechanics,'' in *The Cochlea*, edited by P. Dallos, A. N. Popper, and R. R. Fay (Springer-Verlag, New York), pp. 186–257.
Patuzzi, R., and Robertson, D. (**1988**). ''Tuning in the mammalian cochlea,'' Physiol. Rev. **68**, 1009–1082.
Pfeiffer, R. R. (**1970**). ''A model for two-tone inhibition of single cochlear nerve fibers,'' J. Acoust. Soc. Am. **48**, 1373–1378.
Prijs, V. F. (**1989**). ''Lower boundaries of two-tone suppression regions in the guinea pig,'' Hear. Res. **42**, 73–82.
Recio, A., Narayan, S. S., and Ruggero, M. A. (**1996**). ''Wiener-kernel analysis of basilar membrane responses to noise,'' in *Diversity in Auditory Mechanics*, edited by E. R. Lewis, G. R. Long, R. F. Lyon, P. M. Narins, C. R. Steele, and E. Hecht-Poinar (World Scientific, Singapore), pp. 325–331.
Recio, A., Rich, N. C., Narayan, S. S., and Ruggero, M. A. (**1998**). ''Basilar-membrane responses to clicks at the base of the chinchilla cochlea,'' J. Acoust. Soc. Am. **103**, 1972–1989.

Rhode, W. S. (**1971**). ''Observations of the vibration of the basilar membrane in squirrel monkeys using the Mossbauer technique,'' J. Acoust. Soc. Am. **49**, 1218–1231.
Rhode, W. S. (**1977**). ''Some observations on two-tone interaction measured with the Mossbauer effect,'' in *Psychophysics and Physiology of Hearing*, edited by E. F. Evans and J. P. Wilson (Academic, London), pp. 27–38.
Rhode, W. S., and Cooper, N. P. (**1993**). ''Two-tone suppression and distortion production on the basilar membrane in the hook region of cat and guinea pig cochleae,'' Hear. Res. **66**, 31–45.
Rhode, W. S., and Cooper, N. P. (**1996**). ''Nonlinear mechanics in the apical turn of the chinchilla,'' Aud. Neurosci. **3**, 101–120.
Robert, A., and Eriksson, J. L. (**1999**). ''A composite model of the auditory periphery for simulating responses to complex sounds,'' J. Acoust. Soc. Am. **106**, 1852–1864.
Robles, L., Ruggero, M. A., and Rich, N. C. (**1991**). ''Two-tone distortion in the basilar membrane of the cochlea,'' Nature (London) **349**, 413–414.
Rose, J. E., Hind, J. E., Anderson, D. J., and Brugge, J. F. (**1971**). ''Some effects of stimulus intensity on response of auditory nerve fibers in the squirrel monkey,'' J. Neurophysiol. **34**, 685–699.
Rosowski, J. J. (**1996**). ''Models of External- and Middle-Ear Function,'' in *Auditory Computation (Springer Handbook of Auditory Research, Vol. 6)*, edited by H. L. Hawkins, T. A. McMullen, and A. N. Popper (Springer, New York), pp. 15–61.
Ruggero, M. A., and Rich, N. C. (**1987**). ''Timing of spike initiation in cochlear afferents: Dependence on site of innervation,'' J. Neurophysiol. **58**, 379–403.
Ruggero, M. A., Rich, N. C., Recio, A. (**1996**). ''The effects of intense acoustic stimulation on basilar-membrane vibrations,'' Aud. Neurosci. **2**, 329–346.
Ruggero, M. A., Rich, N. C., Recio, A., Narayan, S. S., and Robles, L. (**1997**). ''Basilar-membrane responses to tones at the base of the chinchilla cochlea,'' J. Acoust. Soc. Am. **101**, 2151–2163.
Ruggero, M. A., Robles, L., and Rich, N. C. (**1992**). ''Two-tone suppression in the basilar membrane of the cochlea: Mechanical basis of auditory-nerve rate suppression,'' J. Neurophysiol. **68**, 1087–1099.
Russell, I. J., Cody, A. R., and Richardson, G. P. (**1986**). ''The responses of inner and outer hair cells in the basal turn of the guinea-pig cochlea and in the mouse cochlea grown in vitro,'' Hear. Res. **22**, 199–216.
Sachs, M. B., and Abbas, P. J. (**1974**). ''Rate versus level functions for auditory-nerve fibers in cats: Tone-burst stimuli,'' J. Acoust. Soc. Am. **56**, 1835–1847.
Sachs, M. B., and Abbas, P. J. (**1976**). ''Phenomenological model for two-tone suppression,'' J. Acoust. Soc. Am. **60**, 1157–1163.
Sachs, M. B., and Kiang, N. Y. S. (**1968**). ''Two-tone inhibition in auditory-nerve fibers,'' J. Acoust. Soc. Am. **43**, 1120–1128.
Schalk, T. B., and Sachs, M. B. (**1980**). ''Nonlinearities in auditory-nerve fiber responses to bandlimited noise,'' J. Acoust. Soc. Am. **67**, 903–913.
Schoonhoven, R., Prijs, V. F., and Frijns, J. H. M. (**1998**). ''Transmitter release in inner hair cell synapses: A model analysis of spontaneous and driven properties of cochlear nerve fibers,'' Hear. Res. **113**, 247–260.
Schwid, H. A., and Geisler, C. D. (**1982**). ''Multiple reservoir model of neurotransmitter release by a cochlea inner hair cell,'' J. Acoust. Soc. Am. **72**, 1435–1440.
Shera, C. A., and Guinan, Jr., J. J. (**2000**). ''Reflection-emission phase: A test of coherent reflection filtering and a window on cochlear-tuning,'' Abstracts of the 23rd Midwinter Meeting of the Association for Research in Otolaryngology, 157.
Smith, R. L. (**1988**). ''Encoding of sound intensity by auditory neurons,'' in *Auditory Function: Neurobiological Bases of Hearing*, edited by G. M. Edelman, W. E. Gall, and W. M. Cowan (Wiley, New York), pp. 243–274.
Teich, M. C., and Lachs, G. (**1979**). ''A neural-counting model incorporating refractoriness and spread of excitation. I. Application to intensity discrimination,'' J. Acoust. Soc. Am. **66**, 1738–1749.
Temchin, A. N., Rich, N. C., and Ruggero, M. A. (**1997**). ''Low-frequency suppression of auditory nerve responses to characteristic frequency tones,'' Hear. Res. **113**, 29–56.
Weiss, T. F., and Rose, C. (**1988**). ''A comparison of synchronization filters in different auditory receptor organs,'' Hear. Res. **33**, 175–180.
Westerman, L. A., and Smith, R. L. (**1985**). ''Rapid adaptation depends on the characteristic frequency of auditory nerve fibers,'' Hear. Res. **17**, 197–198.
Westerman, L. A., and Smith, R. L. (**1988**). ''A diffusion model of the transient response of the cochlear inner hair cell synapse,'' J. Acoust. Soc. Am. **83**, 2266–2276.
Wiederhold, M. L. (**1986**). ''Physiology of the olivocochlear system,'' in *Neurobiology of Hearing: The Cochlea*, edited by R. A. Altschuler, R. P. Robbin, and D. W. Hoffman (Raven, New York), pp. 349–370.
Winter, I. M., and Palmer, A. R. (**1991**). ''Intensity coding in low-frequency auditory-nerve fibers of the guinea pig,'' J. Acoust. Soc. Am. **90**, 1958–1967.
Yates, G. K., Johnstone, B. M., Patuzzi, R. B., and Robertson, D. (**1992**). ''Mechanical preprocessing in the mammalian cochlea,'' Trends Neurosci. **15**, 57–61.
Young, E. D., and Barta, P. E. (**1986**). ''Rate responses of auditory nerve fibers to tones in noise near masked threshold,'' J. Acoust. Soc. Am. **79**, 426–442.
Zagaeski, M., Cody, A. R., Russell, I. J., and Mountain, D. C. (**1994**). ''Transfer characteristic of the inner hair cell synapse: Steady-state analysis,'' J. Acoust. Soc. Am. **95**, 3430–3434.
Zhao, H. B., and Santos-Sacchi, J. (**1999**). ''Auditory collusion and a coupled couple of outer hair cells,'' Nature (London) **399**, 359–362.